Spectroscopic Ellipsometry on Thin Films of TiO_2:

Comparing Cauchy and Cody-Lorentz Models in CompleteEASE

By: Joseph Kreb

An undergraduate thesis

Advised by Dr. Janet Tate

Submitted to the Department of Physics, Oregon State University

In partial fulfillment of the requirements for the degree in BSc in Physics

Submitted on May 31st, 2020

Table of Contents

List of Figures

Abstract

Spectroscopic ellipsometry (SE) is used to characterize amorphous and crystalline thin films of TiO_2. Amorphous precursor films of TiO_2 are deposited by radio frequency magnetron sputtering on fused silica and silicon substrates. Annealing the amorphous precursor films induces them to crystallize into either pure or mixed phases of the three crystal polymorphs of TiO_2: rutile, brookite, and anatase. Previous research in our group has shown that TiO_2 crystal polymorph formation post-annealing, in both pulsed-laser deposition (PLD) and radio frequency magnetron sputtered deposition, is dependent on the thickness of the deposited film, among other deposition parameters.

A set of thin film samples has been made at varying sputtered deposition parameters. SE was employed to estimate the thickness and optical constants of the TiO_2 films. The samples were measured on the wavelength range of 200 – 1000 nm (ultraviolet to near-infrared) with a Woollam M-2000X spectroscopic ellipsometer. The modeling software CompleteEASE was used for data acquisition, and to fit the measured Ψ & Δ spectra with two different optical dispersion models. A Cauchy function models the films as transparent on the restricted wavelength range of 400 – 1000 nm. A Cody-Lorentz oscillator function models the dispersion of the films from 200 – 1000 nm, yielding an estimate of the bandgap energy. Results of fitting model parameters from the two different CompleteEASE models were compared to each other.

Acknowledgements

I am extremely grateful to the many people who are responsible for enabling my scientific education which has led to the production of this undergraduate physics research thesis. My dear parents gifted me with a life of love, support, and quality, such that I could pursue a higher education in physics. My sister convinced me to move from NH to OR to begin going to college at Central Oregon Community College (COCC) in Bend, OR, which set me on this path which I am now completing. I am eternally grateful to her, and my brother, for their support, love, and humor in those first years of my undergraduate education we were together.

Studying physics means a great deal to me and has changed my life in profound ways. I feel very fortunate to have been introduced to physics by professors who study physics education research, and apply the tenets of that research to the design of their courses. I feel that I have been given a high quality education in a difficult subject by these professors, and I thank each of them for their tireless efforts and passion in teaching each of the students who pass before them.

Dr. Wendi Wampler instructed me through my first physics courses at COCC. Her passion for quality of physics education and for the subject itself were infectious and convinced me to switch my major from mathematics to physics, a decision which I am very happy with. At Oregon State University (OSU), I was thrilled to find Wendi's standard of physics education met if not exceeded by the instruction that I received from Dr. Liz Gire in a number of courses. I owe Dr. Giree an indelible debt of gratitude for the intense personal attention and support she gave me, as she tirelessly gives to many students, during my time at OSU. She and Dr. Wampler, both of whom research physics education, are exceptionally dedicated and effective instructors.

I am also extremely grateful to my physics research professor, Dr. Janet Tate for the many opportunities and lessons that she has afforded me personally and in her research group. She has been extremely supportive of me in the completion of this undergraduate physics research thesis, and in the performance of work for her research group, the Tate Labs. I have felt very lucky to work for such a consummate professional and distinguished scientist, and have looked to her as a role model in physics.

I would also like to thank Dr. Doug Keszler of the OSU Chemistry Dept., and his graduate students Jennie Amador and Nizan Kenane for allowing me access to and training me in using the M-2000 X spectroscopic ellipsometer and CompleteEASE. James Hilfiker, of the Woollam company, also helped explain the details of optical modeling in CompleteEASE.

1. Introduction

Spectroscopic ellipsometry (SE) is a well-established optical technique that is commonly used to characterize thin films. The primary objective of this thesis was to use SE to measure the film thickness and optical constants of amorphous and crystalline thin films of Titanium Dioxide (TiO_2). A J.A. Woollam M-2000X spectroscopic ellipsometer was used to measure ψ and Δ spectra of the films, and the modeling software CompleteEASE was used to build and fit optical models to the SE data. Two different CompleteEASE models were developed and fit to the SE data: a Cauchy equation that modeled the films as transparent between 400 – 1000 nm, and a Cody-Lorentz oscillator equation which accounted for the absorption of the bandgap region over the wavelength range of 200 – 1000 nm. The results of these two models were compared to evaluate the consistency of modeling results.

TiO_2 is widely studied for its useful material properties and has many technological and commercial applications. It is a wide band gap, transparent semi-conductor with a high refractive index and a high dielectric constant. Crystalline TiO_2 has three polymorphs: rutile, brookite, and anatase. Brookite is understudied compared to rutile, which is the low-energy, stable crystalline phase (polymorph); brookite and anatase are meta-stable phases. Figure 1 is a diagram from Ref. [1] that shows the crystalline structures of rutile, brookite, and anatase:

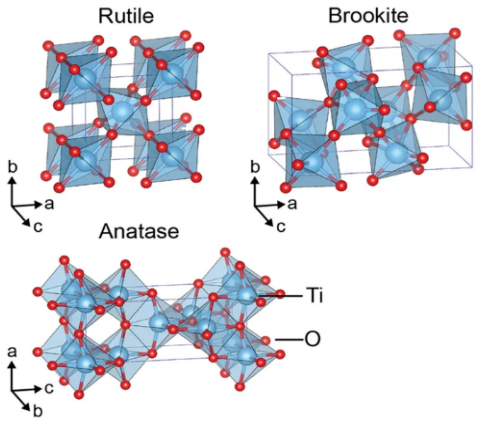

Figure 1: Diagram showing the crystal lattice structure of the different polymorphs of TiO_2. Rutile and anatase have tetragonal crystal structures, while brookite has an orthorhombic crystal structure. Brookite has a larger cell volume than either rutile or anatase Ref. [1].

Our research group has been investigating methods of synthesizing and stabilizing the various polymorphs of thin films of TiO_2. Amorphous (non-crystalline) precursor TiO_2 films were previously deposited by pulsed-laser deposition (PLD) onto substrates of both fused silica (pure

fused SiO_2) and silicon (Si), as in Refs. [1] and [2]. Annealing the films in an oven induces the amorphous precursor films to crystallize into one of the three crystal polymorphs of TiO_2: rutile, brookite, or anatase. Previous graduate students of the Tate research group, James Haggerty and Okan Agirseven, investigated how the pressure of oxygen (pO2) in the PLD chamber and the deposited film thickness influenced which polymorph a precursor film crystallized into when annealed. Figure 2 is a graph from Ref. [2], an article co-authored by Agirseven, that shows the effect of deposition parameters in PLD deposition of TiO_2 films on crystal polymorph formation post-annealing:

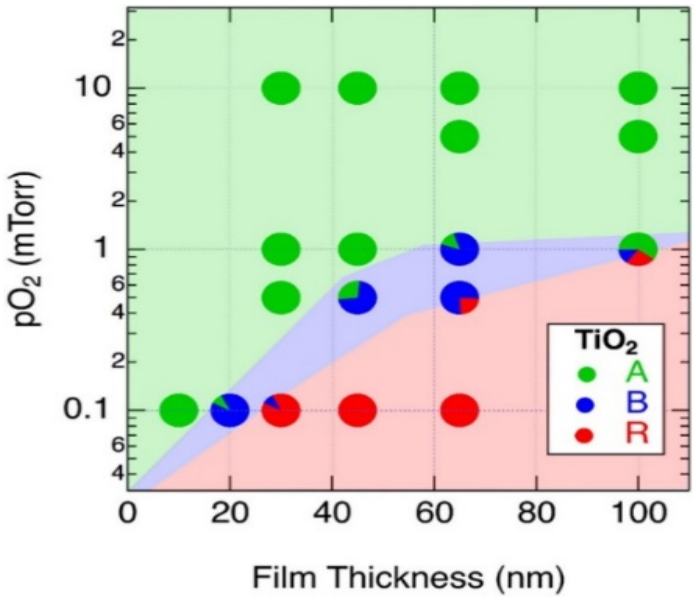

Figure 2: Graph illustrating the dependency of crystal polymorph formation post-annealing on the pressure of oxygen (pO_2) in the PLD deposition chamber and the film thickness. Red, blue and green signify the rutile, brookite, and anatase polymorphs respectively. Notice how brookite only exists in a thin band in the center and how it is easier to crystallize films of rutile or anatase by PLD in comparison.

As can be seen in Figure 2, crystal polymorph formation of TiO_2 films post-annealing was shown to depend on the thickness of the deposited film. Following this discovery, Agirseven began to further explore the dependence of film thickness on polymorph formation in a series of films that he deposited by radio frequency magnetron sputtering. I was employed with the task of learning and utilizing SE to estimate the film thickness and the optical constants of this new set of sputter-deposited thin film samples. Agirseven has deposited these films at various film thicknesses and deposition rates, to explore the role of those two deposition factors in polymorph formation post-annealing.

The primary objective of my assignment was to learn SE and employ it to accurately estimate the thickness of the sputtered TiO_2 films, so that our research group could make conclusions about the effect of film thickness on crystal polymorph formation post-annealing. However, there were other questions that I was capable of addressing and exploring with SE.

We had evidence from electron probe micro analysis (EPMA) that suggested that the films were contracting by perhaps a nanometer or two when annealed. However, this trend in the EPMA data was affected by the fact that we were originally using the same density for amorphous films and each of the polymorphs. The crystal polymorphs rutile, brookite, and anatase have different crystal structures, and different densities. Once we used appropriate densities in the EPMA calculation, the trend in thickness contracting when the films were annealed no longer seemed to occur. We now think that if there is a thickness change from pre- to post-annealed, that it is negligible, if it is occurring at all. SE was used to address the question of change in film thickness pre- to post-annealing in this thesis.

SE also enabled me to estimate the refractive index of the films. I expected the amorphous precursors to all have identical indices, no matter which polymorph they annealed to. I expected to measure a difference in the index for different crystal polymorphs of TiO_2 and a set of films that were pure phase (100% rutile, brookite, or anatase) were measured to have their indices compared. The refractive index of phase pure samples at the sodium yellow emission wavelength of $\lambda = 589$ nm are compared to corresponding estimates obtained using density functional theory in Ref. [3]. I expected to measure refractive indices to be ordered in magnitude from high to low in the following way: rutile, brookite, anatase, amorphous.

It was also a secondary goal of this thesis from the start to compare results from SE with results from intensity-based reflection & transmission spectroscopy that was done by my fellow physics undergraduate, Cameron Stewart. In Stewart's undergraduate thesis work for our group, he measured the reflection and transmission spectra of our TiO_2 films using a grating spectrometer and a silicon detector. Stewart then fit the reflection spectra with projections from a Sellmeier model, in a procedure that is similiar to my fitting of Ψ and Δ spectra with a Cauchy and Cody-Lorentz model. The Sellmeier model lives in an Excel workbook developed in our group to model our films which is called IndexCalc. Fitting the Sellmeier model in IndexCalc yields TiO_2 film thickness and refractive index measurements, as does my method.

In February 2020, Okan Agirseven authored an article from our research group that was published online in the AIP Advances Journal for which I was a listed co-author. In that article,

Agirseven reported on the group's findings regarding polymorph formation of the sputter-deposited TiO_2 films. I am listed as a coauthor for having contributed film thickness estimates from SE, which are compared in the article to estimates from EPMA. The TiO_2 films that were measured for that article were on silicon substrates, and the modeling results from SE are listed in Table A2 in Appendix A. The AIP Advances article itself is listed as Ref. [4].

2. Theory

Ellipsometry is an optical technique that measures the change in the polarization state of light upon reflection from the surface of a material. The way that the polarization of light changes upon reflection from a film depends on the film's thickness and optical properties. The change in polarization of reflected light is measured over a range of wavelengths in spectroscopic ellipsometry (SE). The change in polarization, ρ, is represented by two measurable parameters: Ψ(λ) and Δ(λ). A spectroscopic ellipsometer measures Ψ and Δ spectra.

Due to multiple reflections inherent in thin film systems, there is no simple relationship between Ψ, Δ, *n*, κ, (defined in the next sections) and the film thickness; for this reason, a regression model is used to fit model projections to the experimentally derived Ψ & Δ spectrum data (Ref. [5]). In this experiment, the modeling software CompleteEASE was used to build optical models of the TiO_2 thin film systems. Model fit parameters (namely, the film thickness and optical constants) are adjusted until the model projections of Ψ & Δ spectra closely match the experimentally measured Ψ & Δ spectra. The closeness of the fit is measured by the mean square error (MSE), essentially an average of the difference between experimental values and model values of Ψ & Δ. A low MSE corresponds to a good fit.

If the model is prudently developed, and model parameters are fit to reduce MSE so that the model corresponds with the experimental data, then those parameters closely mirror their true physical values. It is in this way that SE "measures" the film thickness and optical constant values; in truth they are estimations as parameters like film thickness are not directly measured.

2.1 – Interaction of Light with Matter

When light encounters a boundary between two media, some of the light reflects from the boundary and some transmits through. The light that is transmitted into the new medium has its' path deflected by some angle (refracted) according to Snell's Law of refraction:

$$\tilde{n}_1 \sin(\theta_i) = \tilde{n}_2 \sin(\theta_t). \qquad (1)$$

where θ_i is the angle from normal to the interface surface of the incident light path and θ_t is the angle from normal of the transmitted light path, which has been refracted to a different angle based on the refractive index *n*.

The transmitted light also has its phase velocity altered according to the refractive index of the new medium per equation 2:

$$v = \frac{c}{n}. \quad (2)$$

where v is the speed of the light in the material with refractive index n and c is the speed of light in vacuum (c ~ 300,000,000 $\frac{m}{s}$).

The transmitted light may also experience absorption, where the intensity of the light decreases in proportion to the depth, d, into the material that the light travels and the absorption coefficient, α, according to Beer's Law:

$$I(d) = I_0 e^{-\alpha d}. \quad (3)$$

The absorption coefficient is proportional to the extinction coefficient, κ:

$$\kappa = \frac{\lambda}{4\pi}\alpha \quad (4)$$

and the refractive index and extinction coefficient together are the components of the complex index of refraction, $\tilde{n}$, which encapsulates this information about how light interacts with a given material, of a given index of refraction. n and κ are also referred to as the optical constants:

$$\tilde{n} = n + i\kappa. \quad (5)$$

The phrase "optical constants" is a misnomer however, because the value of the refractive index n is proportional to the wavelength of the light in dispersive materials. Optical dispersion is a phenomenon where the phase velocity of light depends on its wavelength. Dispersion is what causes white light to split into a rainbow when it passes through a prism. Since refractive index is a function of wavelength, $n(\lambda)$, the different colors of light (which have different wavelengths) refract through the material at different angles (according to Snell's law) and thus separate into the rainbow.

2.2 – Optical Dispersion Models

Three functions that model the optical dispersion of the TiO_2 films were used or are referenced in this thesis: the Cauchy, Sellmeier and Cody-Lorentz functions. In this thesis, I used Cauchy and Cody-Lorentz models in the modeling software CompleteEASE and compared the results of fitting the parameters of those models to measured Ψ & Δ spectra. Cameron Stewart fit a Sellmeier equation in his fitting of transmission spectra for his thesis work, and it is for that reason that the Sellmeier equation is defined here.

Cauchy function

The Cauchy function (described by equations 6 & 7) is often used to model normal dispersion in the visible wavelength range (roughly 400 – 800 nm) of transparent materials. The function is determined by the Cauchy coefficients A, B, and C, for a given material.

$$n(\lambda) = \mathrm{A} + \frac{\mathrm{B}}{\lambda^2} + \frac{\mathrm{C}}{\lambda^4} \qquad (6)$$

$$\kappa(\lambda) = 0 \qquad (7)$$

The coefficient A largely determines the amplitude of the index and B and C affect the curvature of $n(\lambda)$ across the wavelength spectrum. The Cauchy and Sellmeier equations are used to model a wide variety of materials on a range of wavelengths where they are transparent (Ref. [6]).

Sellmeier function

The Sellmeier function is an improvement made on the Cauchy equation to account for its failures to model dispersion correctly outside of the visible wavelength range. The Sellmeier coefficients to be found for a given material will be referred to here as D and E, in order to distinguish them from the Cauchy coefficients. The Sellmeier equation is:

$$n^2(\lambda) = 1 + \Sigma \frac{\mathrm{D}\lambda^2}{\lambda^2 - \mathrm{E}}. \qquad (8)$$

Cody – Lorentz function

The Cody-Lorentz function was designed to primarily model amorphous semiconductors and dielectrics. For information on the equations and theory at play in the Cody-Lorentz function, look to reference [6]. The benefit, for this thesis, of the Cody-Lorentz function is that it defines a bandgap energy $\mathrm{E_g}$.

2.3 – Reflection of Light from a Surface

In this thesis, reflective spectroscopic ellipsometry was used; ellipsometry can also be done with transmitted light. Light is reflected from specular (uniform) surfaces according to the specular law of reflection:

$$\theta_\mathrm{i} = \theta_\mathrm{r} \, . \qquad (9)$$

There is symmetry to the geometry of the reflection. We describe the polarization of light as having components in two separate planes and these two planes of polarization are based on the geometry of the reflected ray. The incident and reflected ray form a plane, and the

component of the electric field that oscillates in that plane is called the p-plane polarization (p stands for parallel). The electric field oscillation in the direction perpendicular to that is called the s-plane polarization (s stands for “senkrecht”, the German word for perpendicular). The p- and s-plane polarizations are depicted in Figure 3:

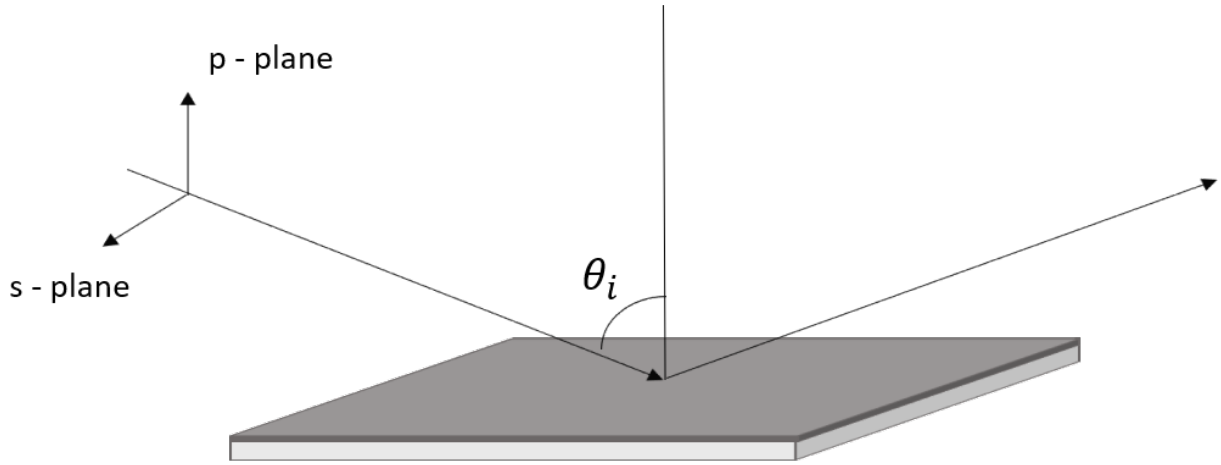

Figure 3: A diagram created by the author that depicts the orientation of the p- and s-plane polarizations. The incident and reflected rays form the p-plane, which is perpendicular to the sample surface. The s-plane polarization is parallel to the sample surface. The gray sample surface represents a TiO_2 film atop the white fused silica substrate.

The amplitude of the electric field changes upon reflection from a surface according to the Fresnel equations for the reflection coefficients in the different planes of polarization:

$$r_p = \frac{\tilde{n}_2 \cos(\theta_i) - \tilde{n}_1 \cos(\theta_t)}{\tilde{n}_2 \cos(\theta_i) + \tilde{n}_1 \cos(\theta_t)} \qquad (10a)$$

$$r_s = \frac{\tilde{n}_1 \cos(\theta_i) - \tilde{n}_2 \cos(\theta_t)}{\tilde{n}_1 \cos(\theta_i) + \tilde{n}_2 \cos(\theta_t)} \qquad (10b)$$

These equations only describe reflection from one surface, however. The samples measured in this thesis are thin films of TiO_2 which range in thickness from ~5 nm to ~ 200 nm. The TiO_2 films are deposited on 1 mm thick substrates of either fused silica or silicon. There are therefore two layers in our samples: the TiO_2 film and the substrate. To account for multiple interfaces, we define the total reflection coefficients in terms of the film phase thickness, β:

(11a)

$$R_p = \frac{r_{12}^p + r_{23}^p e^{-i2\beta}}{1 + r_{12}^p + r_{23}^p e^{-i2\beta}}$$

$$R_s = \frac{r_{12}^s + r_{23}^s e^{-i2\beta}}{1 + r_{12}^s + r_{23}^s e^{-i2\beta}} \qquad (11b)$$

$$\beta = 2\pi \left(\frac{d}{\lambda}\right) \tilde{n}_2 \cos(\theta_2) \qquad (12)$$

Where r_{12}^p refers to the Fresnel reflection coefficient at the interface between medium 1 and medium 2, for p-plane polarized light and *d* is the thickness of the layer. Ellipsometry measures the total reflection coefficients, which are the sum of the initial reflection as well as the internal reflections which are transmitted in turn. The rays that reflect internally before transmitting out of the boundary experience a phase change so that the overall reflected light has a phase change relative to the incident light. Medium 1, 2, and 3 would refer to air, TiO_2, and a substrate of either SiO_2 or Si in this work, as shown in Figure 4:

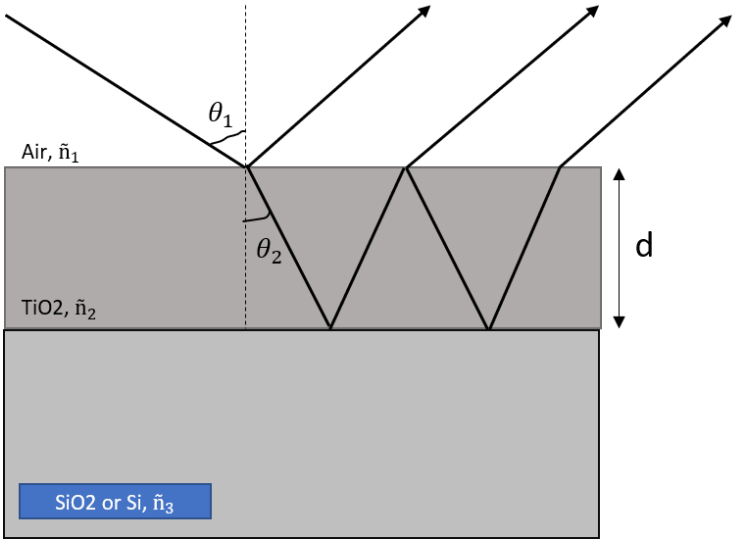

Figure 4: A schematic diagram that depicts internal reflections due to multiple interfaces. The proportions of this diagram are not an accurate representation; in our samples, the films are approximately 1/100 the thickness of the substrate. In the thin films systems measured in this thesis, there is a thin film of TiO_2 (varying in thickness from <5 nm to 150+ nm) atop a substrate of either fused silica or silicon (1 mm thick).

2.4 – Ellipsometry: Detecting the Change in Polarization Upon Reflection

Light is modeled as a transverse electromagnetic wave. When we discuss light we typically speak primarily of the electric field, which at any point in time is described as a vector with some magnitude and pointing in some orientation in space, that oscillates in some manner

over time. If we observe the shape that the electric field traces in a plane perpendicular to propagation, then it may trace a line, circle, or ellipse. This is known as linearly, circularly, or elliptically polarized light, and it is from elliptically polarized light that ellipsometry gets its name.

Light undergoes a change in amplitude and phase upon reflection from a surface. The phase change is not necessarily the same for s and p-plane polarizations. Therefore, linearly polarized light, with s and p-plane polarization components has its amplitudes and phases change differently, resulting in elliptically polarized light. This is where ellipsometry gets its name. In ellipsometry, light of a known linear polarization state is reflected off the surface of a sample and the change in the polarization to elliptically polarized light is measured. The central equation of ellipsometry is:

$$\rho = \frac{R_p}{R_s} = \tan(\Psi)e^{i\Delta}. \qquad (13)$$

The change in polarization of the light upon reflection, ρ, is physically measured as the ratio of the total reflection coefficients. This ratio is parameterized with two variables to represent the amplitude change, Ψ, and the phase shift, Δ:

$$\tan(\Psi) = \frac{|R_p|}{|R_s|} \qquad (14)$$

$$\Delta = \delta_1 - \delta_2 \qquad (15)$$

where δ_1 is the phase difference between the s and p-plane polarized light for the incident light ray and δ_2 is the same phase difference but for the outgoing, reflected light ray. SE measures Ψ and Δ as functions of wavelength, Ψ(λ) and Δ(λ), also called Ψ and Δ spectra.

The objective of SE is to closely "fit" experimentally measured Ψ and Δ spectra with projected curves from a model of the system that is being measured. An optical model is built with adjustable parameters such as film thickness and value of the optical constants. These are referred to as the model fit parameters. When the model projections of Ψ & Δ closely replicate the measured SE data (Ψ and Δ spectra), then the model fit parameters closely approximate their real physical values. In this way, we estimate the film thickness and optical constants and do not directly measure it. The degree to which a model is closely "fitting" the data is gauged by using the mean square error (MSE) estimator.

MSE averages the root of the squares of the difference between real values and model values. When this difference is minimized, the model values are close to the real values and the

model is closely fitting the data. When this occurs, the model fit parameters are closely approximating their true, physical values.

$$\mathrm{MSE_{NCS}} = \sqrt{\frac{1}{3n-m}\sum_{i=1}^{n}\left(\frac{\mathrm{N_{E_i}} - \mathrm{N_{G_i}}}{0.001}\right)^2 + \left(\frac{\mathrm{C_{E_i}} - \mathrm{C_{G_i}}}{0.001}\right)^2 + \left(\frac{\mathrm{S_{E_i}} - \mathrm{S_{G_i}}}{0.001}\right)^2} \qquad (16)$$

where *n* is the number of data points and *m* is the number of fit parameters. N, C and S are entries in the Mueller matrix, which is an optics concept that is relevant to ellipsometry but does not need to be discussed in detail here. N, C and S are related to Ψ and Δ in the following way:

$$\mathrm{N} = \cos(2\Psi) \qquad (17)$$

$$\mathrm{C} = \sin(2\Psi) \qquad (18)$$

$$\mathrm{S} = \sin(2\Psi)\sin(\Delta) \qquad (19)$$

Measuring MSE in terms of N, C, and S is analogous to measuring MSE in terms of difference in the Ψ and Δ of the measured SE data and model projections. References [7] and [8] were used for the development of this theory section.

3. Methods

3.1 – J.A. Woollam M-2000X Spectroscopic Ellipsometer

The Ψ and Δ spectra of our TiO_2 films were measured with an M-2000X model spectroscopic ellipsometer made by the J.A. Woollam Co., Inc. This model of ellipsometer has a patented rotating analyzer that measures all wavelengths simultaneously for very quick measurement; data acquisition time is a few seconds. The sample stage and polarizer/analyzer arms are motorized to translate to different positions and incident angles. The light source is a 75W Xenon lamp, which emits a broadband spectrum in the ultraviolet to near-infrared wavelength range (200 – 1000 nm). Figure 5 is a picture of the M-2000X ellipsometer at its current home: The Advanced Technology and Manufacturing Institute (ATAMI) in Corvallis, Oregon:

Figure 5: The M-2000X spectroscopic ellipsometry system used in these results (pictures taken by author). The polarizer and analyzer arms (left and right, respectively) are pointed down at the sample stage in the center.

3.2 – CompleteEASE v.6.54

The Woollam company's M-2000X ellipsometer was run in conjunction with their proprietary data acquisition and modeling software, CompleteEASE version 6.54. This software works with the ellipsometer and is used to select data acquisition parameters for measurement of Ψ and Δ spectra, as well as to build and fit optical models of measured samples to those

spectra. Figure 6 shows CompleteEASE open to the Analysis tab, where model building and fitting is done on SE data. In Figure 6, the SE data for sample # 44, pre-annealed is open and displayed in the Variable Angle Spectroscopic Ellipsometric (VASE) Data window. The CompleteEASE Cauchy model, defined in section 3.2.2., is being applied to the data, and the result is a good fit. As can be seen in Figure 6, the model projections (dashed lines) lie closely over the measured Ψ & Δ spectra (red and green lines, respectively), with a low MSE of 2.781.

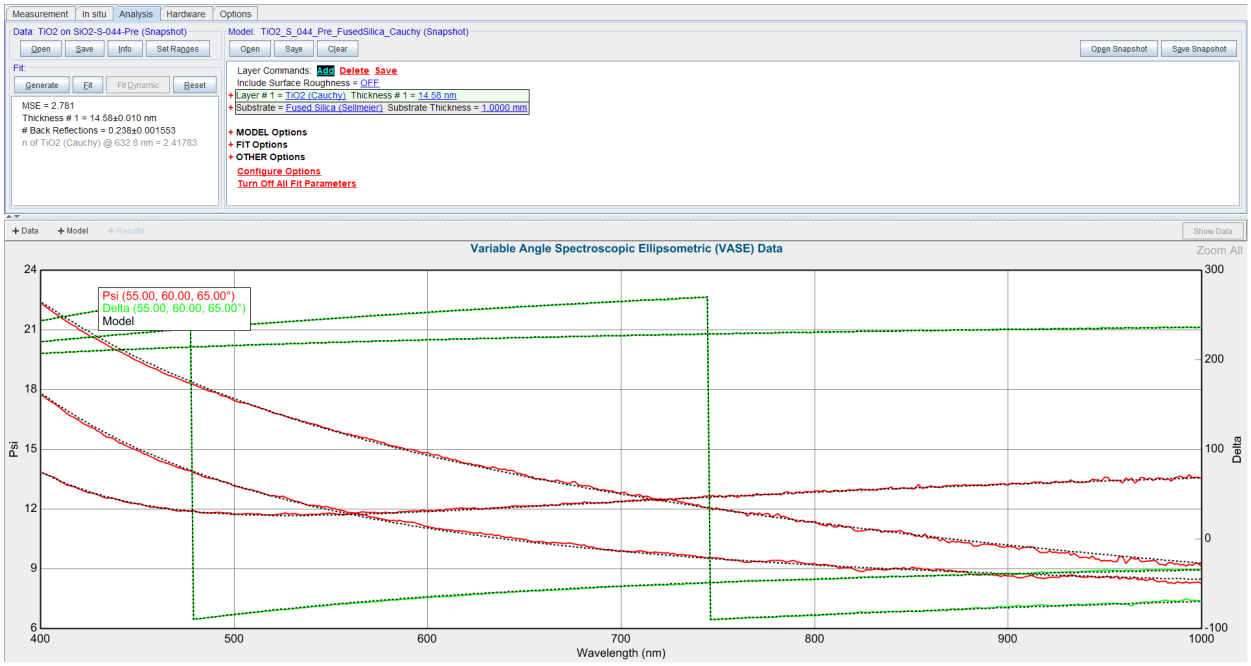

Figure 6: CompleteEASE displaying the Analysis tab, where layer optical models are developed. The Ψ & Δ spectra of sample #44 pre-annealed are displayed in the VASE Data window. The CompleteEASE Cauchy model for fused silica substrates is open and being applied, resulting in an MSE of 2.781, as seen in the Fit window.

Every SE measurement in this thesis was made with the same data acquisition parameters. Ψ & Δ spectra were measured at three incident angles (55°, 60°, 65°). Since two parameters, Ψ and Δ, are measured at each incident angle, the result is six curves in the VASE Data window, as seen in Figure 6. High accuracy mode was used for measurements of TiO_2 films on fused silica substrates. These films are mostly transparent on the measured wavelength range, and coupled with the transparent fused silica substrates produce a weak reflection signal that is accounted for by the high accuracy mode. Measurements were made with a single point scan pattern and a data acquisition time of 4 seconds.

The CompleteEASE manual (Ref. [8]) is an excellent general reference on how to use CompleteEASE prudently for various types of modeling. A user guide to CompleteEASE with

specific information and advice on how CompleteEASE was used in the modeling of the TiO_2 films measured in this thesis was written by the author. This guide is found in Appendix B, labeled as CompleteEASE User Reference Guide.

3.2a – CompleteEASE substrate models

Optical models of each of the two types of substrate (fused silica and silicon) were chosen from selections in the available databases in CompleteEASE:

The fused silica substrate was modeled with the "Fused Silica (Sellmeier).mat" model. Figure 7 shows the expanded window view of the Fused Silica (Sellmeier).mat model:

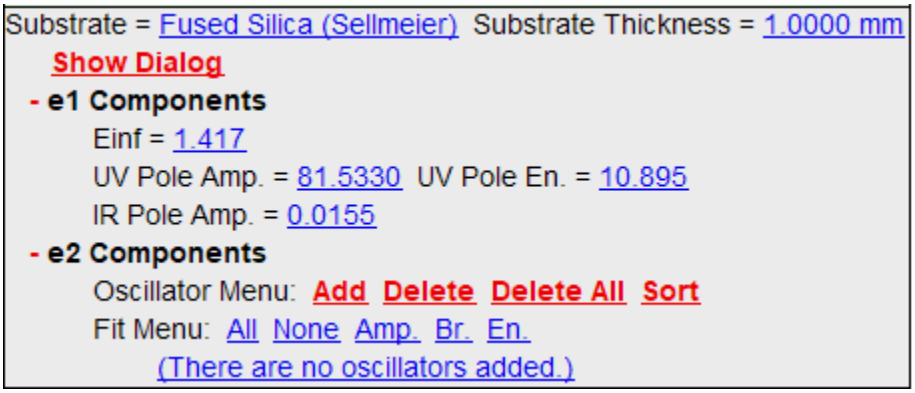

Figure 7: Fused Silica (Sellmeier).mat model used to model the fused silica substrate of our TiO_2 films. The model fit parameters of the substrate were kept at the above, initial values of the model for all results in this thesis.

The model fit parameters of the substrates were not fitted, or allowed to alter from their initial values, as the substrates are ideally identical between different TiO_2 films.

The silicon substrate was modeled with the "Si_JAW.mat" model. This model of silicon has no fittable model parameters, so there is no expanded window view.

3.2b – CompleteEASE Cauchy model

The TiO_2 films were modeled in CompleteEASE with an available Cauchy model called, "TiO_2 (Cauchy).mat". Figure 8 shows the expanded window view of the TiO_2 (Cauchy).mat model, with the Fused Silica (Sellmeier) substrate model applied:

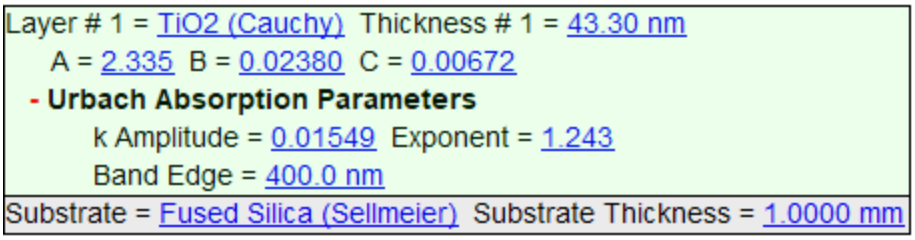

Figure 8: The TiO_2 (Cauchy).mat model used to model thin films of TiO_2 as transparent in the visible wavelength range, in this case with the fused silica substrate. The model fit parameters are at their initial values.

The model fit parameters are the values in blue in the model which can be changed, apart from band edge and substrate thickness, which were kept at the above values. The model fit parameters are "fit" or adjusted by using a standard, iterative, non-linear regression algorithm (the Levenberg-Marquardt method) to automatically reduce the MSE by altering the fit parameters. This Cauchy model was used on the restricted wavelength range 400 – 1000 nm, which is visible to near infrared, though the ellipsometer measured Ψ & Δ spectra on the range of 200 – 1000 nm. The wavelength was restricted in this way because a Cauchy equation is not designed to model the absorption of the bandgap, which in the case of TiO_2 is approximately 3.2 eV (3.2 eV corresponds to a wavelength of ~ 387 nm).

The Cauchy model for the TiO_2 layer was used to model films on both fused silica and silicon substrates.

3.2c – CompleteEASE Cody-Lorentz model

The TiO_2 films were also modeled in CompleteEASE with a Cody-Lorentz model called, "TiO_2 (CodyLor).mat". Figure 9 shows the expanded window view of this model:

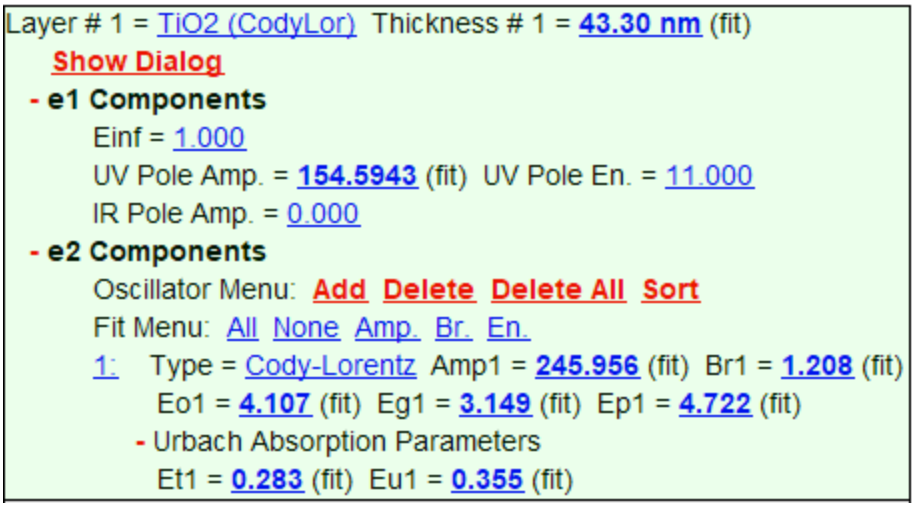

Figure 9: The TiO_2 (CodyLor).mat model used to model TiO_2 films in CompleteEASE. The parameters of the model which were fitted are highlighted in dark blue with (fit) next to them. All other model parameters were kept at their initial values, as shown above.

This model was used over the full measured wavelength range of 200 – 1000 nm, as it does account for the absorption of the bandgap, with a Cody-Lorentz oscillator model. For a fulsome description of the Cody-Lorentz function and the model fit parameters, refer to Ref. [6]. The Cody-Lorentz model has the advantage of providing estimates of the bandgap energy, E_g, of the TiO_2 films.

The modeling methods employed in CompleteEASE were informed by a series of articles in Vacuum Technology & Coating on the subject of characterizing thin films of materials in CompleteEASE. These articles are references [5] and [10 – 14].

4. Results

4.1 – Tables of Fitted Parameters from CompleteEASE Models

The Ψ and Δ spectra of sixty-eight thin films of TiO_2 on fused silica substrates and nineteen TiO_2 films on silicon substrates were measured using an M-2000X spectroscopic ellipsometer. The Ψ & Δ spectra of these films were then fit in CompleteEASE with one of two options developed to model the TiO_2 film: the CompleteEASE Cauchy or Cody-Lorentz models. Depending on the substrate of the film being modeled, the Fused Silica (Sellmeier) or Si_JAW.mat models were used (for fused silica and silicon substrates, respectively). The results of fitting model parameters for the films are contained in Tables A1 – A4, found in Appendix A.

Table A1 lists an important subset of fitted model parameters for the sixty-eight films on fused silica substrates that includes:

- Sample identification number, MSE, TiO_2 film thickness (nm), refractive index at 633 nm, and band gap energy (Eg1) from the Cody-Lorentz model

Table A2 lists the following fitted model parameters from applying the CompleteEASE Cauchy model to the set of nineteen TiO_2 films on silicon substrates that were measured:

- Sample ID, MSE, TiO_2 film thickness (nm), Cauchy coefficients A, B, and C

Table A3 has the following additional model fitting parameters, not listed in Table 1, from applying the CompleteEASE Cauchy model to the fused silica substrate films:

- Cauchy coefficients A, B, and C, amplitude of the extinction coefficient (k amplitude), and exponent (k amplitude and corresponding exponent are the Urbach absorption parameters defined in this Cauchy model)

Table A4 lists the following model fit parameters from applying the CompleteEASE Cauchy model to a set of nineteen TiO_2 films on silicon substrates on the wavelength range of 400 – 1000 nm:

- Sample ID, MSE, TiO_2 film thickness (nm), and the Cauchy coefficients A, B, and C

4.2 – Correspondence of CompleteEASE Cauchy and Cody-Lorentz Models

Many of the thin TiO_2 films were successfully modeled with both the Cauchy and Cody-Lorentz models. One model did not clearly work better than the other and good results were gained from using both. The Cody-Lorentz model had the advantage of providing an estimate of

the band gap energy, however the Cauchy model is simpler, was more familiar to the author, and can be easier to use and understand. Figure 10 shows how the thicknesses of amorphous films that were estimated by the two different CompleteEASE models compare to one another:

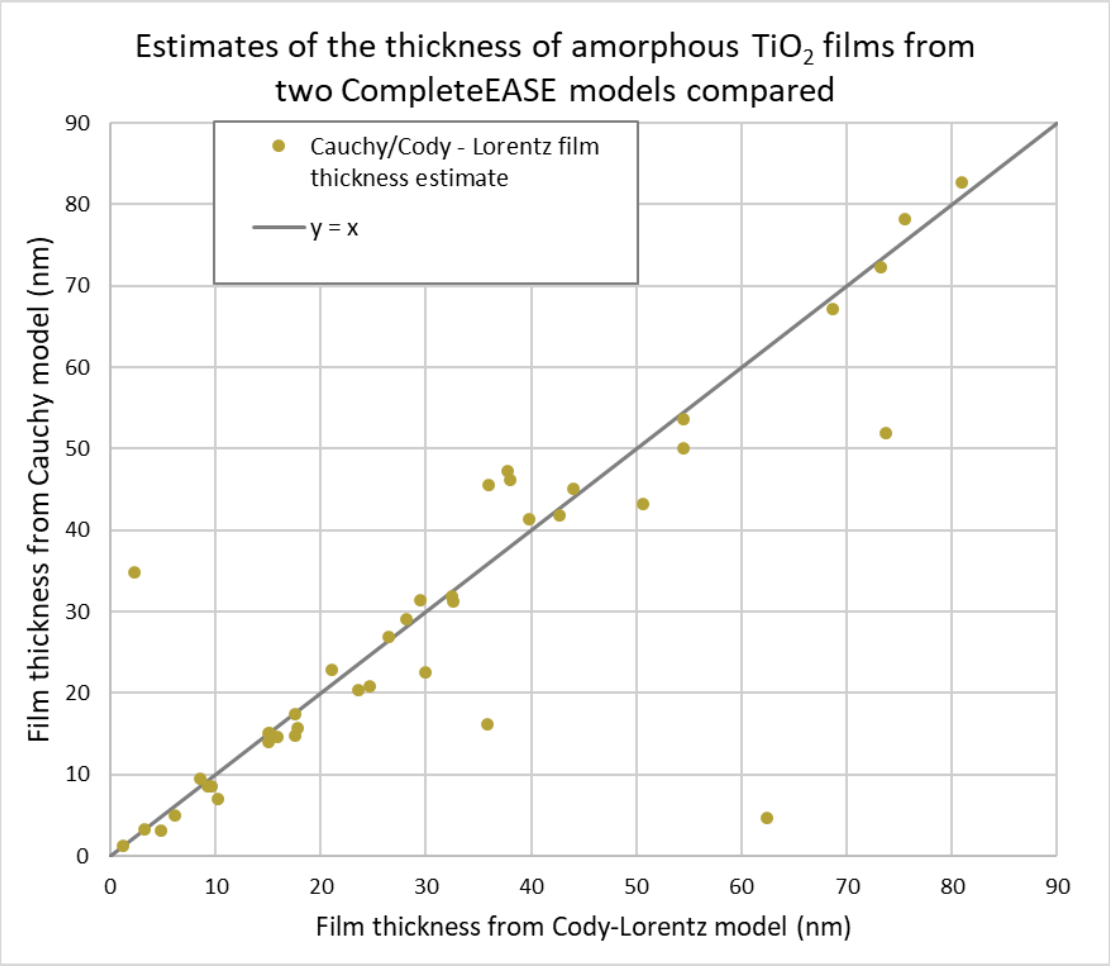

Figure 10: Film thickness from Cauchy model plotted against film thickness from Cody-Lorentz model. The points lie on the line when the models agreed in their thickness estimates. It can be seen that the models were generally in agreement, apart from four significant outliers.

The Cauchy and Cody-Lorentz CompleteEASE generally corresponded well in their estimates of the thickness of the TiO_2 films, apart from four outlying cases. Figure 11 shows the correspondence between estimates of the refractive index at 633 nm of the TiO_2 films between the two CompleteEASE models. Figure 11 shows a clustering of datapoints around a refractive index of approximately 2.4 at 633 nm for the amorphous films. It was expected that we would measure a distinct refractive index for all of the amorphous films, and this clustering around a

single value serves as evidence of the fact that amorphous films do not differ in index, not matter what crystal polymorph they anneal to.

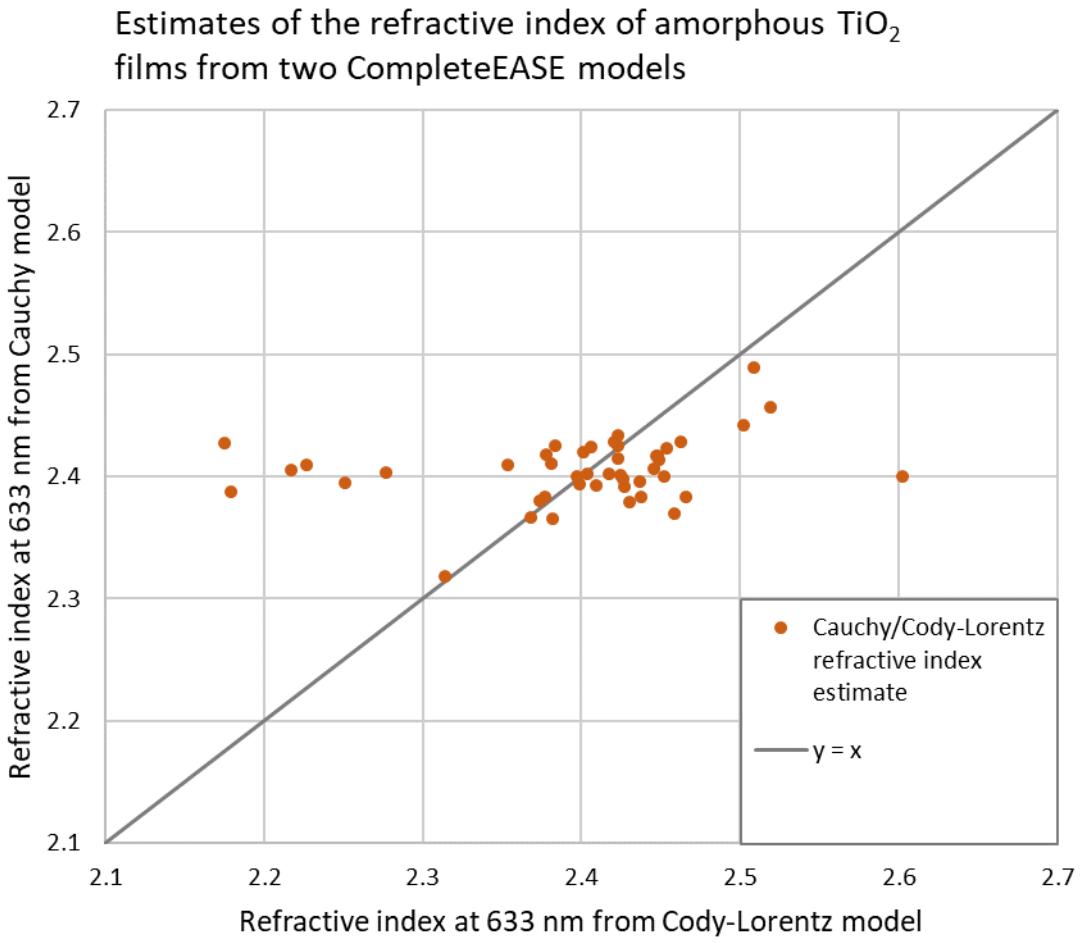

Figure 11: Correspondence of refractive index at 633 nm from Cauchy and Cody-Lorentz CompleteEASE models. The models did not seem to agree as well in refractive index estimates as they did with film thickness estimates. The magnitude of the refractive index of amorphous TiO_2 films appears to cluster around a value of ~ 2.4. There are 7 significant outliers in this correspondence that. The most extreme outliers differ by about 8% in their estimates.

4.3 – Change in TiO_2 Films from Amorphous to Crystalline

Change in film thickness

We had evidence from EPMA to suggest that the films were contracting by a few nanometers when annealed. From the results of modeling with SE, it is difficult to point to any trend in the change in film thickness upon annealing. Some films seemed to contract from modeling results, while others seemed to expand. The modeling does not seem to have been

done well enough to yield estimates of film thickness that are precise enough to establish a definitive trend. Generally, the films seemed to decrease in thickness by a few nanometers when annealed, although examples to the contrary can be found in the results.

Table 1 shows thickness changes from pre- to post-annealed for six of the best modeled films on silicon substrates. The full modeling results for these can be found in Table A2, in Appendix A:

Sample ID	Pre-annealed MSE	Post-annealed MSE	TiO2 film thickness change, pre to post-annealed (nm)
9	0.988	1.579	+ 0.22
12	0.546	0.361	+ 1.07
22	0.506	0.0962	- 0.99
30	6.789	6.152	+ 1.46
32	1.277	2.145	+ 3.61
36	0.16	0.0553	+0.04

Table 1: TiO_2 film thickness change from pre- to post-annealed for six films on silicon substrates. There is no clear trend in the change in film thickness from pre to post. The best modeled film, sample #36, suggests that the change in film thickness is negligible, if occurring at all.

Table 2 shows thickness changes from pre- to post-annealed for five of the best modeled films on fused silica substrates. Each of these are from results of the CompleteEASE Cauchy model; the full list of such results is contained in Table A1 in Appendix A. This table of results also shows no definitive trend in the change in film thickness upon annealing.

Sample ID	Pre MSE	Post MSE	TiO2 film thickness change, pre to post-annealed (nm)
42	2.162	1.29	+ 0.3
44	2.781	6.632	- 0.95
50	1.161	1.296	+ 0.07
55	2.2	2.634	- 5.08
80	1.428	1.984	- 0.79

Table 2: TiO_2 film thickness change from pre- to post-annealed for five films on fused silica substrates. These are results from the CompleteEASE Cauchy model. There is no clear trend in the change in film thickness from pre to post. The best modeled film in this list, sample #50, suggests that the change in film thickness is negligible, if occurring at all.

Change in refractive index

The general trend of the refractive index increasing upon annealing into crystalline films was established, as can be seen in Figure 12, which lists the refractive indices of a set of four films on fused silica substrates modeled with the CompleteEASE Cauchy model:

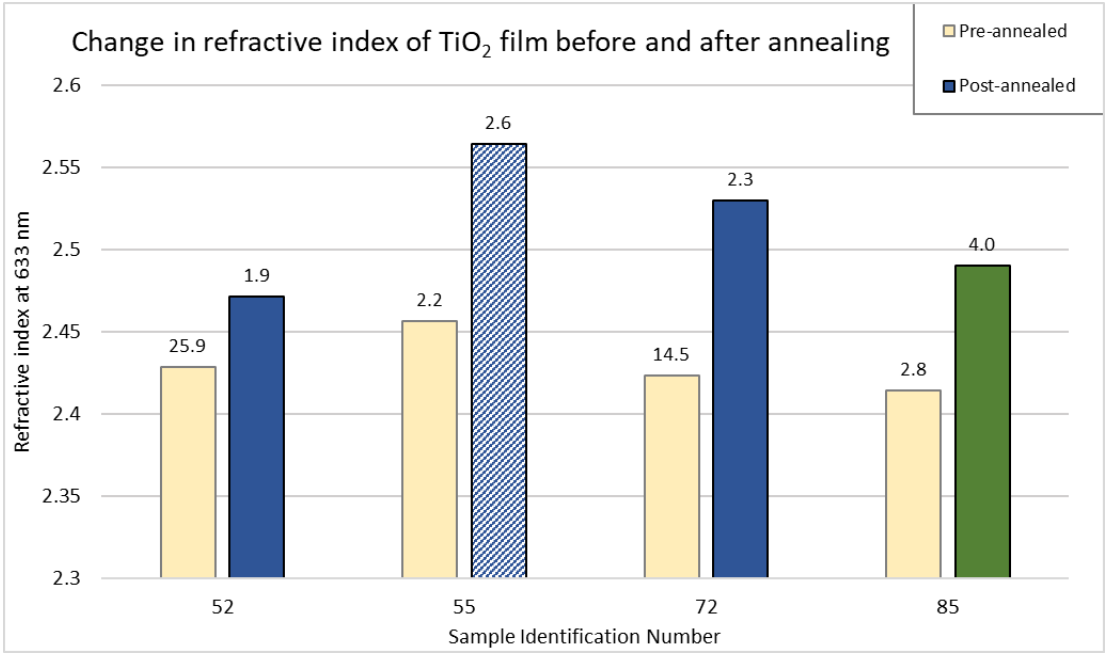

Figure 12: Refractive index increasing from pre- to post-annealed films modeled with the CompleteEASE Cauchy model. The refractive index of the amorphous TiO_2 films was found to be ~2.4, while the index of the three polymorphs were higher, and distinct from one another. The numbers at the top of each column are the corresponding MSE of the model fits.

4.4 – Refractive Index of Crystalline TiO_2 Films

A subset of TiO_2 films were targeted for measurement in the post-annealed, crystalline state due to the distribution of polymorphs (rutile, brookite, or anatase) that they attained when annealed. Figure 13 shows estimates of the refractive index from applying the CompleteEASE Cauchy and Cody-Lorentz model to a subset of nine crystalline TiO_2 films, followed by Table 3, which lists the crystal phase fractions of each sample as determined by EPMA:

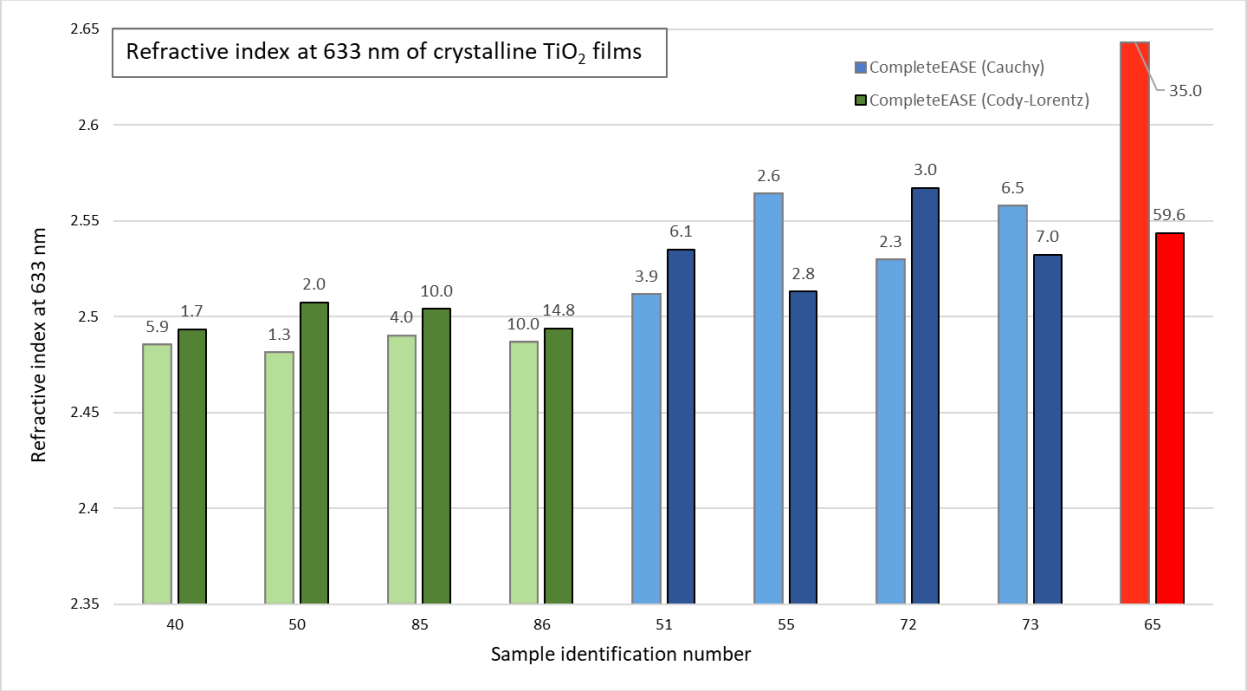

Figure 13: Graph showing the refractive index at 633 nm of crystalline TiO_2 films modeled in CompleteEASE. The Cauchy model results are in a lighter color than the Cody-Lorentz model results. The MSE of the model fit is listed at the top of each column. Anatase, brookite, and rutile films are color-coded as green, blue, and red, respectively. The difference in magnitude of the refractive index of the different crystal polymorphs of TiO_2 is depicted in this graph, with the expected order in magnitude from high to low of rutile, brookite, and anatase.

Table 3 lists the crystal phase fractions for the films listed in Figure 13, in terms of the percentage of each polymorph (anatase, brookite, or rutile) that the film was found to consist of from EPMA measurement by Okan Agirseven:

Sample ID	% Anatase	% Brookite	% Rutile
40	100	-	-
50	95	5	-
85	100	-	-
86	100	-	-
51	-	95	5
55	47	53	-
72	-	99.85	0.15
73	3.75	95.75	0.5
65	-	-	100

Table 3: Crystal polymorph distributions from EPMA of the nine TiO_2 films featured in Figure 14.

Figure 13 shows the expected order in magnitude of refractive index for the crystal polymorphs of TiO_2 with rutile the highest, followed by brookite and then anatase (Ref. [3]). Figure 13 also serves to show some of the discrepancy that exists between the two CompleteEASE models. This is particularly notable in the case of sample #55, which has a low MSE on both models, but the refractive index is estimated to be noticeably different. This set of nine films are the best modeled films that had available phase distribution information from EPMA.

Reference [3] is a published paper that calculated the refractive index of rutile, brookite, and anatase from first principles calculations. The authors of that paper calculated the refractive index of rutile, brookite, and anatase at 589 nm in two ways, one of which was using the Gladstone-Dale (GD) equation. The other method used in Ref. [3] was density functional theory, however I will choose the GD equation estimates of refractive index to compare my SE results to. The GD and density functional theory estimates of refractive index are close enough that I chose to use one instead of considering both. The results of applying the GD equation in Ref. [3] were refractive indices at 589 nm of 2.56, 2.65, and 2.70 for anatase, brookite, and rutile, respectively.

Estimates of the refractive index of polymorphs of TiO_2 from SE done in this thesis are consistently lower in magnitude by a few hundredths than the estimates from [3] that use the GD equation, as shown in Table 4:

Sample ID	n at 589 nm, CompleteEASE Cauchy	n at 589 nm, CompleteEASE Cody-Lorentz	n @ 589 nm, Gladstone-Dale [3]
40	2.50770	2.51796	2.56
50	2.50813	2.53220	2.56
85	2.51816	2.52351	2.56
86	2.51501	2.52031	2.56
51	2.53354	2.55830	2.65
72	2.55510	2.59198	2.65
73	2.58349	2.55709	2.65
65	2.68282	2.56557	2.70

Table 4: Comparing estimates of refractive index at 589 nm from two CompleteEASE models and an external source, Ref. [3]. The SE index estimates differ from the Ref. [3] by no more than 5%. Sample ID are color coded: green, blue and red for pure phase anatase, brookite, and rutile samples, respectively.

The refractive index estimates from SE are all lower than from Ref. [3], however the difference is not significant. The most extreme difference is the result for sample #65 from the Cody-Lorentz model and from Ref. [3] (2.56557 compared to 2.70, respectively), which amounts to a ~5% difference. The estimate of refractive index from SE done in this thesis for every other sample in the table above is closer to its respective expected value from [3]. It is interesting to note that in Ref. [3], it is mentioned how the GD equation is typically accurate to within 5% for minerals. Sample #55 is not included in Table 2 as it is a mixed phase film.

4.5 – Comparison of CompleteEASE and IndexCalc Modeling Results

As discussed previously, fellow physics undergraduate Cameron Stewart performed intensity-based reflection and transmission spectroscopy on our TiO_2 film samples. He then fit the reflection spectra with a Sellmeier equation in an Excel workbook called IndexCalc. Readers are encouraged to reference Cameron's thesis for more details on his procedure. Cameron and I measured some films in common, and sought to compare the results of modeling with the two CompleteEASE models to that from IndexCalc. Figure 14 shows the estimates of thickness (in nm) of the TiO_2 film from the three models for a set of seven pre-annealed films that we measured in common:

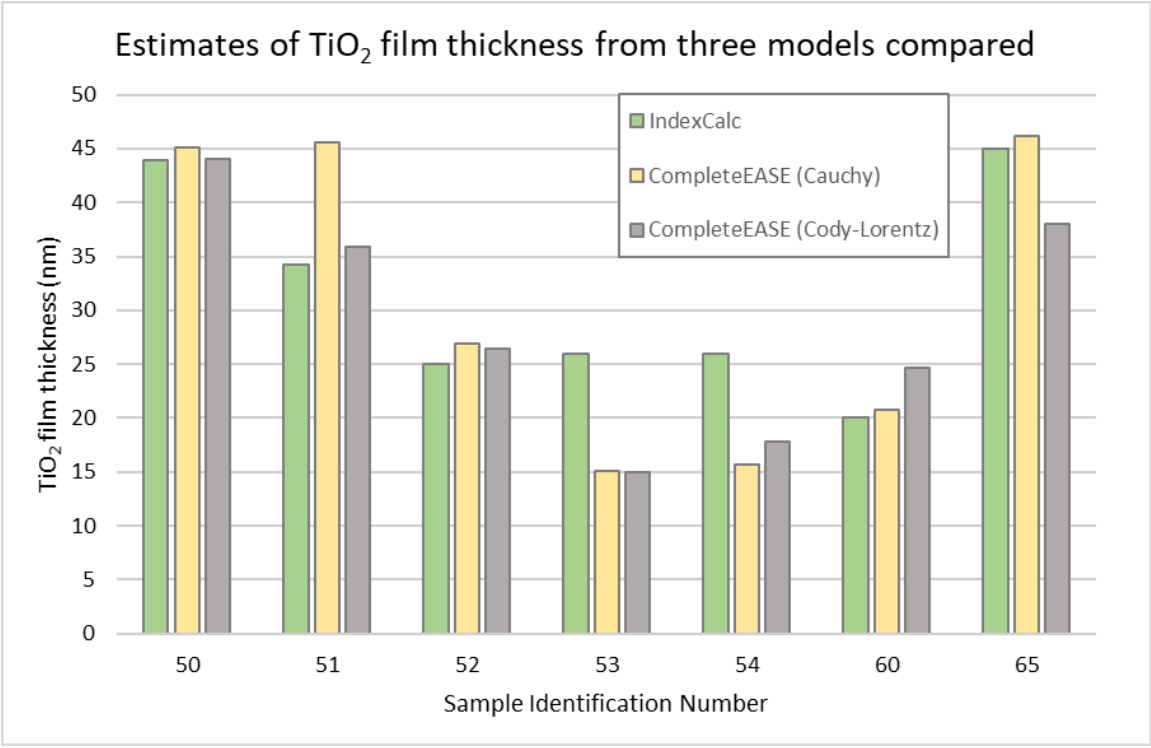

Figure 14: Estimates of the thickness of the TiO_2 film from IndexCalc and the two CompleteEASE models developed for this thesis compared. These seven films are all in the amorphous, pre-annealed state.

Figure 15 shows the estimates of the refractive index at 633 nm of the TiO_2 film for a set of post-annealed, crystalline films that Cameron and I both measured. The three models (IndexCalc, and the CompleteEASE Cauchy and Cody-Lorentz models) agree much more closely in their estimates of the refractive index of the films in Figure 15 than they agree on the film thicknesses in Figure 14. There is variability in the results of each of the models that makes it difficult to know what the exact film thicknesses or refractive indices are, to an exacting detail.

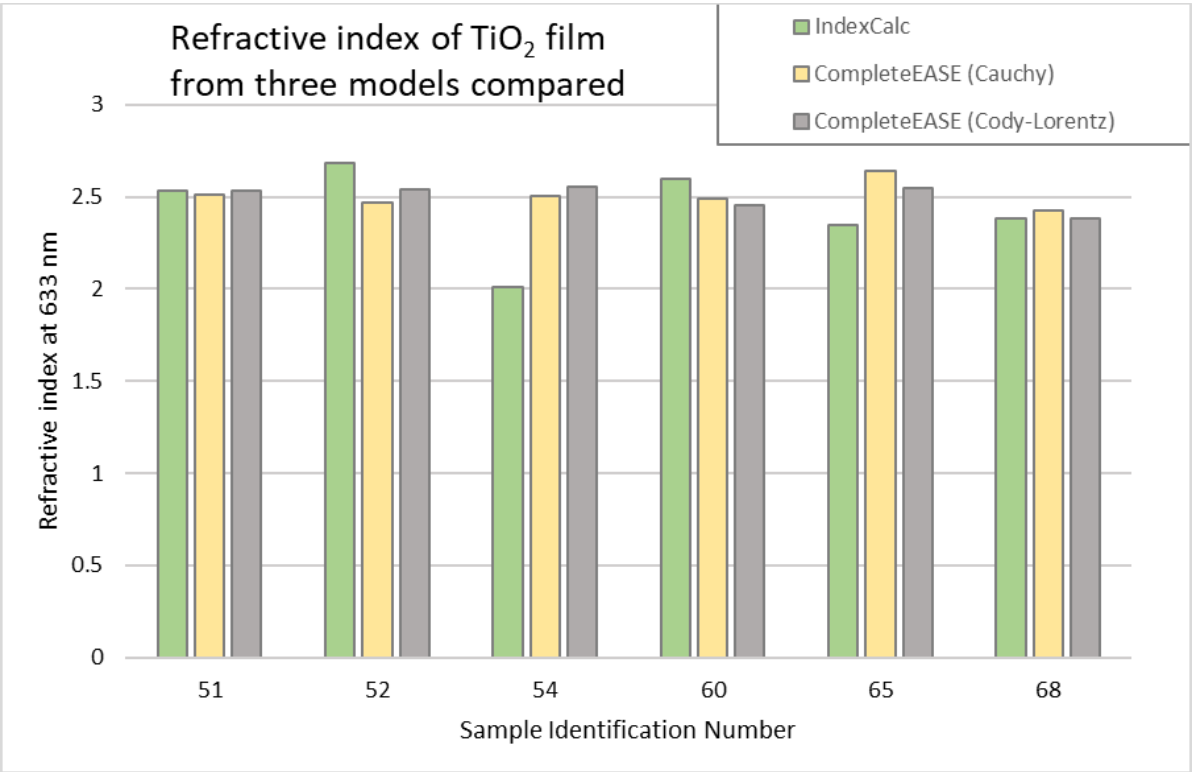

Figure 15: Estimates of the refractive index at 633 nm of six crystalline TiO_2 films from IndexCalc and the two CompleteEASE models developed for this thesis compared. As can be seen, there is close agreement between the models for these films. The most notable discrepancy is the result of the IndexCalc model for sample #54.

5. Conclusion

The Ψ and Δ spectra of sixty-eight TiO_2 films on fused silica substrates and nineteen TiO_2 films on silicon substrates were measured using a M-2000X spectroscopic ellipsometer. The Ψ and Δ spectra were then fit with optical models developed in CompleteEASE. A Cauchy model was developed in CompleteEASE that modeled the films as mostly transparent on the wavelength range of 400 – 1000 nm. In addition, a Cody-Lorentz oscillator model was developed in CompleteEASE to include modeling of the bandgap of the TiO_2 films (and provide an estimate of the band gap energy) on the wavelength range of 200 – 1000 nm.

Both CompleteEASE models were successful in modeling our TiO_2 films and extracting meaningful data, especially estimates of the film thickness which are very useful in our research group. The models were shown to generally correspond with each other, as in Figures 10 and 11, which showed that the estimates of TiO_2 film thickness and refractive index at 633 nm were mostly the same between the two models, apart from a few outlying cases in either figure. However, there appeared to be variability in the modeling results for film thicknesses, which is reflected in Figure 14 which shows the discrepancies that exist between thickness estimates, even between the two CompleteEASE models.

The author was more familiar with the Cauchy model, and therefore those results are likely to be overall better and more reliable than the Cody-Lorentz model results. Table A1 can be consulted to find the discrepancy between CompleteEASE modeling results for all of the measured films. It is estimated that film thickness results may vary by plus or minus a few nanometers. This variability can be significant in the case of films that are ~ 40 nm, as many of the measured films are. Films that were below 20 nm, or greater than 100 nm were difficult to model, and therefore the estimates of film thickness for such films is not as reliable as films that are around 40 nm thick.

No clear trend could be established as to how the thickness of the TiO_2 films changed when annealed. Some of the best modeled results in Tables 1 and 2 suggest that there is a negligible increase in film thickness of a few hundredths of a nanometer. Many films with higher MSE fits showed a decrease by ~ 1 nm or more from pre to post, but other results showed an increase in film thickness. The inconsistency of the results means that no clear trend can be stated. However, there was a clear and expected trend in the refractive index increasing from pre- to post-annealed films, as shown in Figure 12.

The amorphous, pre-annealed films were found to have a similar, low refractive index, as evidenced in Figure 11, which shows a clustering around a magnitude of ~ 2.4 for the index of amorphous films at 633 nm. The expected ordering of refractive index magnitude between amorphous and crystalline films was also found to exist, and is shown in Figure 12. The indices can be ordered from high to low in the following way: rutile, brookite, anatase, and amorphous (as expected from Ref. [3]). In general, it appears that the refractive indices were estimated with better precision than the film thicknesses.

The refractive index at 589 nm of phase pure crystalline films of rutile (sample #65), brookite (samples #51, #55, #72, #73), and anatase (samples #40, #50, #85, #86) were found to be within 5% of estimates from Ref. [3], which used a Gladstone-Dale equation and mass densities to estimate the refractive index of those TiO_2 polymorphs.

Finally, results from SE were compared with Cameron Stewart's IndexCalc estimates from applying a Sellmeier equation to fit the reflection spectra of the TiO_2 films. Figure 14 shows variability in the estimates of TiO_2 film thickness between the three models being compared. This figure also shows that the two CompleteEASE models were not consistent for these films. Figure 15 compares the estimates of refractive index for the same set of films between the three models, and shows a much closer agreement in the results. This serves as further evidence that the film thicknesses do not appear to have been as precisely estimated as the refractive indices.

Greater emphasis should have been placed on refining the models so that the best fits were available for all of the measured films. The MSE for many fits is higher than would be publishable. An MSE of greater than 10 for the CompleteEASE Cauchy and Cody-Lorentz models is not ideal, though some samples are higher than this. The only measured pure phase rutile film had a very high MSE in both CompleteEASE models. In addition, it proved difficult to accurately model the film thickness of very thin films (less than 20 nm) or thick films (greater than 100 nm), although the intent in the group was to vary the film thickness and see how it affected polymorph formation post-annealing.

Still, SE appears to have given us good estimates of the film thickness and refractive index of these set of sputter-deposited TiO_2 films that are useful to our research group. The speed with which SE can acquire data, and the range of options available in optical modeling makes it a valuable resource for characterizing thin films such as ours. Future efforts could be made towards improving modeling so that the estimates of refractive index, and in particular the film thicknesses, are more precise.

References

1. J. E. Haggerty, J. Tate, et al., “High-fraction brookite films from amorphous precursors”, *Scientific Reports* **7**, 15232 (2017).
2. J. S. Mangum, et al., “Selective brookite polymorph formation related to the amorphous precursor state in TiO_2 thin films”, *Journal of Non-Crystalline Solids* ***505****, 109-114 (2019).*
3. X. Rocquefelte, F. Goubin, S Jobic, et al., “Investigation of the Origin of the Empirical Relationship between Refractive Index and Density on the Basis of First Principles Calculations for the Refractive Indices of Various TiO_2 Phases”, *Inorganic Chemistry* **43**, 2246-2251 (2004).
4. O. Agirseven, D. T. Rivella Jr., J. E. S. Haggerty, P. O. Berry, K. Diffendaffer, A. Patterson, J. Kreb, J. Tate, et al., “Crystallization of TiO_2 polymorphs from RF-sputtered, amorphous thin-film precursors”, *AIP Advances* **10**, 025109 (2020).
5. B. Johnson, J. Hilfiker, M. Linford, “Some Fundamentals of Spectroscopic Ellipsometry”, *Vacuum Technology & Coating* **20**, 3 (2019)
6. H. Fujiwara, R. Collins, J. Hilfiker, T. Tiwald, “Chapter 5: Dielectric Function Modeling”, *Spectroscopic Ellipsometry for Photovoltaics Volume 1: Fundamental Principles and Solar Cell Characterization* **1**, pgs. *115 - 153* (2018).
7. R. M. Azzam, N. M. Bashara, “Ellipsometry and Polarized Light” (1977)
8. H. G. Tompkins, “A User’s Guide to Ellipsometry” (1993)
9. [PDF], “CompleteEASE Software Manual, Data Acquisition and Analysis Software for J.A. Woollam Spectroscopic Ellipsometers”
10. T. Avval, B. Johnson, J. Hilfiker, M. Linford, “A Tutorial on Spectroscopic Ellipsometry (SE), 1. Determination of the Thicknesses of Thin Oxide Layers on Semiconductor Substrates”, *Vacuum Technology & Coating* **20**, 4 (2019)
11. D. Shah, D. Patel, J. Hilfiker, M. Linford, “A Tutorial on Spectroscopic Ellipsometry (SE), 2. The Cauchy Model”, *Vacuum Technology & Coating* **20**, 5 (2019)
12. D. Patel, D. Shah, J. Hilfiker, B. Johs, M. Linford, “A Tutorial on Spectroscopic Ellipsometry (SE), 3. Surface Roughness”, *Vacuum Technology & Coating* **20**, 6 (2019)
13. D. Shah, D. Patel, J. Hilfiker, B. Johs, M. Linford, “A Tutorial on Spectroscopic Ellipsometry (SE), 4. Using the ‘Angle Offset’ when fitting Ellipsometric Data”, *Vacuum Technology & Coating* **20**, 7 (2019)

14. D. Patel, D. Shah, J. Hilfiker, M. Linford, “A Tutorial on Spectroscopic Ellipsometry (SE), 5. Using the Tauc-Lorentz and Cody-Lorentz Models to Describe the Absorption features of Amorphous Silicon (a-Si)”, *Vacuum Technology & Coating* **20**, 9 (2019)

Appendix A: Tables of CompleteEASE modeling results

TABLE A1: Subset of CompleteEASE Cauchy and Cody-Lorentz model fitting results for TiO_2 films on fused silica substrates

Table 1 shows a subset of results from fitting both a Cody-Lorentz oscillator and a Cauchy equation in CompleteEASE to Ψ and Δ spectra measured by an M-2000X spectroscopic ellipsometer, as described in the methods. This table lists modeling results for TiO_2 films on fused silica substrates. For each film in this table, there are two rows: the first row reports the Cauchy model results (which don't report an estimate of the band gap energy, Eg), followed by a row that reports the Cody-Lorentz model results (which do have estimates for Eg).

Sample ID	MSE	TiO2 film thickness (nm)	*n* (683 nm) of TiO_2 film	Eg (eV)
30 pre	22.57	78.15	2.4006	
30 pre	23.16	75.53	2.39747	3.177
31 pre	17.39	16.21	2.3871	
31 pre	35.995	35.81	2.17883	3.432
32 pre	3.751	4.67	2.4099	
32 pre	63.235	62.38	2.22682	2.526
32 post	44.66	30.61	2.4968	
32 post	53.97	41.98	2.3766	2.876
36 pre	18.681	20.35	2.4091	
36 pre	12.316	23.62	2.35397	3.392
40 post	5.866	29.93	2.4852	
40 post	1.726	28.49	2.49341	3.226
41 pre	1.44	3.12	2.4269	
41 pre	1.498	4.79	2.17542	3.135
42 pre	2.162	7.03	2.4053	
42 pre	2.668	10.17	2.21692	3.221
42 post	1.29	7.33	2.518	
42 post	2.056	9.29	2.32997	3.526
43 pre	3.801	29	2.3925	

Sample ID	MSE	TiO2 film thickness (nm)	*n* (683 nm) of TiO_2 film	Eg (eV)
43 pre	3.964	28.14	2.4094	3.231
44 pre	2.781	14.58	2.4178	
44 pre	2.238	15.91	2.37767	2.937
44 post	6.632	13.63	2.4631	
44 post	16.928	15.67	2.51098	3.106
46 pre	3.105	3.29	2.4255	
46 pre	7.309	3.3	2.4234	3.36
47 pre	1.125	1.28	2.3976	
47 pre	1.341	1.25	2.42641	3.159
48 pre	5.179	53.56	2.4172	
48 pre	8.553	54.52	2.44693	3.142
49 pre	20.417	43.14	2.3918	
49 pre	75.445	50.58	2.42727	2.657
50 pre	1.161	45.05	2.4896	
50 pre	2.065	44.02	2.50858	3.13
50 post	1.296	45.12	2.4813	
50 post	1.98	43.3	2.50731	3.149
51 pre	31.062	45.55	2.3832	
51 pre	18.012	35.94	2.46588	3.185
51 post	3.858	36.24	2.5116	
51 post	6.092	35.9	2.53506	2.976
52 pre	25.921	26.95	2.4287	
52 pre	14.718	26.47	2.42087	3.191
52 post	1.881	26.9	2.4714	
52 post	2.926	26.22	2.53665	3.209
53 pre	1.974	15.05	2.3664	
53 pre	2.369	15.02	2.3679	3.199
54 pre	30.914	15.64	2.3963	

Sample ID	MSE	TiO2 film thickness (nm)	*n* (683 nm) of TiO_2 film	Eg (eV)
54 pre	14.356	17.78	2.43701	3.204
54 post	3.924	13.29	2.5063	
54 post	6.036	12.95	2.5566	2.753
55 pre	2.2	31.4	2.4565	
55 pre	2.829	29.44	2.51877	3.744
55 post	2.634	26.32	2.5641	
55 post	2.76	29.3	2.51308	3.225
58 pre	31.452	138.78	2.3999	
58 pre	23.79	135.58	2.45182	3.092
58 post	50.397	131.95	2.4811	
58 post	31.468	132.46	2.51141	3.134
59 pre	31.151	47.2	2.36985	
59 pre	18.047	37.77	2.45833	3.198
60 pre	18.56	20.81	2.3937	
60 pre	17.97	24.65	2.39869	3.403
60 post	1.35	21.09	2.4869	
60 post	1.44	22.39	2.45149	3.222
61 pre	11.732	67.13	2.4019	
61 pre	17.663	68.7	2.41726	3.008
61 post	4.438	64.47	2.4975	
61 post	13.567	67.39	2.46477	3.599
62 pre	34.504	271.36	2.40142	
62 pre	34.4	269.05	2.42427	3.157
62 post	34.541	259.13	2.4838	
62 post	35.261	259.54	2.49041	3.16
63 pre	3.494	4.96	2.4033	
63 pre	3.538	6.15	2.27649	3.186
64 post	3.339	67.6	2.5121	

Sample ID	MSE	TiO2 film thickness (nm)	*n* (683 nm) of TiO_2 film	Eg (eV)
64 post	5.475	68.69	2.49149	3.311
65 pre	42.033	46.16	2.3999	
65 pre	23.26	38.01	2.60246	2.836
65 post	35.027	26.85	2.6431	
65 post	59.647	38.79	2.54365	2.927
67 pre	1.469	9.5	2.4147	
67 pre	2.473	8.55	2.42309	2.964
68 pre	9.54	22.91	2.3789	
68 pre	7.007	21.09	2.43039	3.144
69 pre	0.275	14.03	2.4248	
69 pre	3.29	15.09	2.38346	3.131
70 pre	3.116	14.84	2.33955	
70 pre	2.61	17.56	2.25096	3.221
71 pre	15.1	41.74	2.4171	
71 pre	15.469	42.69	2.44811	3.137
72 pre	14.486	31.85	2.4232	
72 pre	18.225	32.52	2.45372	3.129
72 post	2.285	32.57	2.5298	
72 post	3.009	2.23	2.56713	4.038
73 pre	12.171	22.56	2.4104	
73 pre	25.386	29.94	2.38143	3.84
73 post	6.549	25.49	2.5577	
73 post	6.988	26.56	2.53216	3.229
75 pre	7.61	15.14	2.4337	
75 pre	7.384	15.1	2.42312	3.281
76 pre	12.855	50.03	2.3804	
76 pre	15.983	54.42	2.37364	3.089
77 pre	27.546	132.74	2.3831	

Sample ID	MSE	TiO2 film thickness (nm)	*n* (683 nm) of TiO_2 film	Eg (eV)
77 pre	26.027	134.41	2.37689	2.984
77 post	44.523	125.78	2.5344	
77 post	66.004	123.3	2.58329	3.266
78 pre	14.311	31.17	2.4279	
78 pre	16.396	32.6	2.46227	3.206
79 pre	1.462	34.87	2.3832	
79 pre	1.169	2.25	2.43783	4.072
80 pre	1.428	17.46	2.4024	
80 pre	1.493	17.57	2.40333	3.199
80 post	1.984	16.67	2.50576	
80 post	2.883	17.91	2.43996	3.526
81 pre	2.046	8.63	2.4197	
81 pre	4.167	9.66	2.4009	3.006
82 pre	17.913	72.24	2.365	
82 pre	27.858	73.26	2.38215	3.093
82 post	35.057	68.39	2.4985	
82 post	146.9	63.1	2.58847	5.33
83 post	1.756	17.06	2.5497	
83 post	1.991	18.63	2.49782	3.129
85 pre	2.765	41.28	2.4141	
85 pre	1.868	39.8	2.44887	3.133
85 post	4.041	37.01	2.49	
85 post	10.014	39.82	2.50396	3.211
86 pre	27.221	170.82	2.442	
86 pre	33.155	165.54	2.50192	2.995
86 post	9.957	167.14	2.4868	
86 post	14.753	166.96	2.49369	3.028
87 pre	4.758	8.56	2.4246	

Sample ID	MSE	TiO2 film thickness (nm)	*n* (683 nm) of TiO_2 film	Eg (eV)
87 pre	5.3	9.32	2.40585	3.273
88 pre	7.678	82.71	2.4068	
88 pre	3.005	80.92	2.44544	3.333
89 pre	47.052	51.84	2.3186	
89 pre	95.088	73.67	2.31416	15

TABLE A2: Subset of CompleteEASE Cauchy model fitting results for TiO_2 films on silicon substrates

Table 2 shows a subset of modeling results from optically modeling TiO_2 films on silicon substrates in the modeling software CompleteEASE, as discussed in methods. The Cauchy coefficients A, B, and C are reported, as well as the MSE of the fit and the estimated TiO_2 film thickness. A low MSE corresponds to a good fit, and more reliable estimates of model fit parameters. Multiple rows for a sample correspond to multiple instances of applying the Cauchy model and finding different results for model fit parameters, which are all reported.

Sample ID	TiO_2 film thickness (nm)	MSE	A	B	C
9 pre	47.84	5.564	1.359	0.0617	0
	34.89	0.886	2.267	0.00562	0.00977
	35.06	0.988	2.255	0.02374	0.00676
9 post	48.19	5.564	1.238	0.1465	0
	35.28	1.579	2.499	0.0238	0.00695
10 pre	46.65	6.183	1.458	0.0933	0
	32.34	17.123	1.965	0.0237	0.00668
10 post	45.64	6.973	1.535	0.1629	0
	33.5	14.956	2.285	0.001257	0.00614

Sample ID	TiO_2 film thickness (nm)	MSE	A	B	C
12 pre	31.67	0.546	2.226	0.0346	0.0061
12 post	32.74	0.361	2.44	0.0238	0.011
22 pre	24.26	0.506	2.309	0.0254	0.002
	25.05	0.535	2.235	0.02042	0.00669
	25.34	10.713	2.325	0.02333	0.000707
22 post	23.27	0.0962	2.393	0.0121	0.0117
	25.77	0.394	2.352	0.02221	0.00593
	29.45	8.228	2.353	0.02575	0.00681
29 pre	25.49	0.48	2.301	0.0243	0.0024
30 pre	59.27	12.54	2.346	0.0236	0.0134
	69.3	6.789	2.449	0.02795	0.00834
30 post	60.68	10.05	2.315	0.0859	0.0066
	70.76	6.152	2.409	0.02954	0.0076
31 pre	22.37	1.359	2.248	0.0464	0.006
	21.69	0.0958	2.327	0.02521	0.00698
	21.04	20.646	2.285	0.04166	0.00716
	22.488	22.488	2.201	0.04236	0.00722
31 post	23	19.101	2.47	0.02953	0.00743
32 pre	40.1	1.277	2.032	0.091	0.0019
	43.36	13.189	2.255	0.02316	0.00672
32 post	43.71	2.145	2.237	0.091	0.0019
	50.22	20.576	2.48	0.02051	0.00783

Sample ID	TiO_2 film thickness (nm)	MSE	A	B	C
33 pre	5.35	0.102	2.284	0.0108	0
	7.26	0.089	2.053	0.00445	0.00693
33 post	5.81	0.0525	2.401	0.0386	0
	8.14	0.231	2.337	0.01662	0.00876
36 pre	22.79	0.16	2.258	0.024	0.005
36 post	22.83	0.0553	2.281	0.0282	0.007

TABLE A3: Additional CompleteEASE Cauchy model fitting results for TiO_2 films on fused silica substrates

Table 3 lists additional fitted model parameters from applying the CompleteEASE Cauchy model to the sixty-eight TiO_2 films on fused silica substrates that are featured in Table 1, but were not reported in that table. Table 1 was limited to an important subset of model fit parameters from applying both the Cauchy and Cody-Lorentz models to the sixty-eight measured TiO_2 films on fused silica substrates. Table 3 lists as yet unreported model fit parameters for the Cauchy model, and Table 4 does the same for the Cody-Lorentz model. The results in this table are additional parts of the overall modeling results of the sixty-eight Cauchy entries of Table 1.

The Cauchy coefficients A, B, and C are reported in addition to the Urbach absorption parameters of k amplitude and Exponent. The films were modeled as mostly transparent in the wavelength range of 400 – 1000 nm for the Cauchy model, so the k amplitude and exponent often fit to be near or at zero.

Sample ID	MSE	A	B	C	k amplitude	Exponent
30 pre	22.57	2.343	0.00887	0.00564	0.14058	0
31 pre	17.39	2.316	0.00862	0.008	0.31257	0
32 pre	3.751	2.311	0.02398	0.00624	0.12479	1.243
32 post	44.66	2.262	0.07722	0.00665	0.60982	0

Sample ID	MSE	A	B	C	k amplitude	Exponent
36 pre	18.681	2.312	0.01794	0.00846	0.15223	1.3
40 post	5.866	2.387	0.0226	0.00665	0	1.233
41 pre	1.44	2.324	0.02584	0.00618	0.09014	1.114
42 pre	2.162	2.311	0.02008	0.00715	0.10264	0.823
42 post	1.29	2.429	0.01937	0.00652	0.04498	1.285
43 pre	3.801	2.303	0.01922	0.00665	0	0
44 pre	2.781	2.32	0.01961	0.00778	0.11085	0.663
44 post	6.632	2.308	0.04927	0.00521	0.13399	0.627
46 pre	3.105	2.344	0.01456	0.00716	0.09893	0.649
47 pre	1.125	2.295	0.02988	0.00444	0.07192	0.02988
48 pre	5.179	2.32	0.01535	0.0094	0.10579	0
49 pre	20.417	2.291	0.02697	0.00543	0.18008	0
50 pre	1.161	2.358	0.03411	0.0074	0.03049	0.429
50 post	1.296	2.359	0.03142	0.00708	0	1.243
51 pre	31.062	2.328	0.02021	0.00077	0	1.243
51 post	3.858	2.39	0.02549	0.00925	0.06246	0
52 pre	25.921	2.313	0.2886	0.007	0.14106	0
52 post	1.881	2.317	0.04704	0.00584	0.03364	0
53 pre	1.974	2.304	0.000489	0.008	0.00977	0
54 pre	30.914	2.3	0.02004	0.00747	0.10236	0
54 post	3.924	2.378	0.03632	0.006	0.12364	0.433
55 pre	2.2	2.319	0.04179	0.00538	0	1.243
55 post	2.634	2.413	0.04356	0.00673	0.646	0
58 pre	31.452	2.183	0.08554	0.000308	0	1.73E-17
58 post	50.397	2.336	0.01819	0.01595	0.16286	1.243
59 pre	31.151	2.345	0.00011	0.00401	0.00011003	0
60 pre	18.56	2.303	0.01619	0.00813	0.05	0.17
60 post	1.35	2.362	0.03462	0.00617	0.04517	0.772

Sample ID	MSE	A	B	C	k amplitude	Exponent
61 pre	11.732	2.312	0.01656	0.00774	0.15387	0
61 post	4.438	2.374	0.02277	0.01069	0.07211	0
62 pre	34.504	2.297	0.01926	0.009	0.05591	0
62 post	34.541	2.361	0.02799	0.00855	0.06478	0
63 pre	3.494	2.274	0.04027	0.00467	0.0579	1.1
64 post	3.339	2.344	0.05759	0.00392	0.01501	0
65 pre	42.033	2.271	0.02841	0.00934	0.05206	0
65 post	35.027	2.451	0.04483	0.01285	0.44115	0
67 pre	1.469	2.347	0.01016	0.00687	0.03706	0.924
68 pre	9.54	2.285	0.02339	0.0057	0	0.03
69 pre	0.275	2.322	0.02536	0.00629	0.06398	0.64
70 pre	3.116	2.339	0.00376	0.00758	0.06571	0.06571
71 pre	15.1	2.314	0.0254	0.00632	0.17066	0
72 pre	14.486	2.338	0.01701	0.00678	0.1569	0
72 post	2.285	2.419	0.02399	0.00824	0.02148	0
73 pre	12.171	2.313	0.02161	0.007	0.18087	0
73 post	6.549	2.451	0.02173	0.00839	0.06929	0.997
75 pre	7.61	2.348	0.02094	0.00541	0	0.929
76 pre	12.855	2.291	0.02425	0.00467	0.22274	0
77 pre	27.546	2.28	0.02516	0.00652	0.10348	0
77 post	44.523	2.398	0.03725	0.00695	0.07404	0
78 pre	14.311	2.33	0.02134	0.0072	0.13551	0
79 pre	1.462	2.274	0.03885	0.00595	0	1.243
80 pre	1.428	2.291	0.03035	0.0057	0.01037	0
80 post	1.984	2.41	0.02257	0.00635	0.04916	1.806
81 pre	2.046	2.336	0.01171	0.00879	0.07606	0.688
82 pre	17.913	2.277	0.01989	0.00608	0.17271	0
82 post	35.057	2.348	0.04135	0.00765	0.087	0

Sample ID	MSE	A	B	C	k amplitude	Exponent
83 post	1.756	2.403	0.04608	0.00508	0.06353	0.645
85 pre	2.765	2.302	0.0289	0.00637	0	1.821
85 post	4.041	2.362	0.03261	0.00751	0.17066	0.761
86 pre	27.221	2.374	0.01695	0.00417	0.0451	0
86 post	9.957	2.334	0.05062	0.00422	0.02735	0
87 pre	4.758	2.345	0.01827	0.00527	0.05216	0
88 pre	7.678	2.323	0.01623	0.007	0.0053	2.345
89 pre	47.052	2.209	0.02	0.00958	0.43909	0

TABLE A4: Additional CompleteEASE Cody-Lorentz model fitting results for TiO_2 films on fused silica substrates

Table 4 lists additional model fitting parameters from applying the CompleteEASE Cody-Lorentz model to the sixty-eight TiO_2 films on fused silica substrates that are listed in Table 1. The results in this table are additional parts of the overall modeling results of the sixty-eight Cody-Lorentz entries of Table 1.

Sample ID	UV Pole Amp	Amp	Br	Eo	Eg	Ep	Et
30 pre	162.9329	186.752	0.959	4.059	3.177	4.194	0.395
31 pre	226.1427	336.791	3.391	4.217	3.432	7.403	3.078
32 pre	16.6665	88.778	2.875	3.791	2.526	3.206	0.986
32 post	50.1684	225.311	0.95	3.894	2.876	4.77	0.576
33 pre	100.6896	272.421	1.416	4.02	3.311	5.862	0
36 pre	179.8848	75.121	1.833	4.174	3.392	2.077	0
40 post	113.4388	444.625	1.074	4.135	3.226	6.203	0.216
41 pre	63.8205	714.661	1.394	4.087	3.135	10.59	0.318
42 pre	36.1419	910.183	1.383	4.052	3.221	10.525	0.405
42 post	206.8826	68.998	1.495	3.733	3.526	1.251	0.246
43 pre	113.8222	440.14	1.129	4.131	3.231	6.551	0.353

Sample ID	UV Pole Amp	Amp	Br	Eo	Eg	Ep	Et
44 pre	62.4006	745.899	1.306	4.07	2.937	10.371	0.451
44 post	221.4475	174.323	1.063	4.086	3.106	4.284	0.36
46 pre	-40.3766	1000	1.153	4.017	3.36	8.038	0.725
47 pre	53.7056	721.373	1.418	4.114	3.159	8.849	0.359
48 pre	155.6268	234.522	1.416	4.116	3.142	4.941	0.288
49 pre	-25.788	984.224	0.888	2.648	2.657	4.956	0.338
50 pre	143.426	295.177	1.199	4.112	3.13	5.304	0.277
50 post	154.5947	245.954	1.208	4.107	3.149	4.722	0.283
51 pre	201.4482	227.237	1.087	4.073	3.185	4.815	0.401
51 post	172.2419	140.697	1.522	4.153	2.976	3.767	0.242
52 pre	149.9088	238.775	1.045	4.096	3.191	4.784	0.391
52 post	84.9089	795.408	1.161	4.123	3.209	8.38	0.0869
53 pre	137.8814	199.467	1.496	4.053	3.199	4.293	0
54 pre	149.966	234.842	1.32	4.136	3.204	4.812	0.367
54 post	106.8711	715.286	1.208	4.052	2.753	10.463	0.63
55 pre	187.4045	377.828	0.432	3.769	3.744	1.827	0.19
55 post	83.9723	740.763	1.116	4.105	3.225	7.944	0.172
58 pre	125.0236	305.794	1.1	4.028	3.092	5.36	0.262
58 post	154.6826	264.196	1.075	3.942	3.134	4.465	0.242
59 pre	192.1756	228.736	1.14	4.063	3.198	4.752	0.393
60 pre	229.2818	166.126	1.164	4.422	3.403	4.524	0
60 post	90.1705	719.274	1.007	4.125	3.222	8.163	0.173
61 pre	159.925	307.593	1.218	4.178	3.008	6.751	0.471
61 post	186.6257	35.211	2.895	4.35	3.599	0.402	0.267
62 pre	45.8079	286.56	1.228	3.979	3.157	4.447	0.228
62 post	77.1772	358.86	1.092	3.929	3.16	4.862	0.227
63 pre	34.5536	880.627	1.369	4.056	3.186	10.109	0.215
64 post	120.2546	354.235	1.139	4.096	3.311	5.018	0.179

Sample ID	UV Pole Amp	Amp	Br	Eo	Eg	Ep	Et
65 pre	169.5154	222.607	1.114	3.954	2.836	4.808	0.456
65 post	241.3117	203.246	0.989	4.003	2.927	5.017	0.357
67 pre	30.4853	1000	1.377	4.08	2.964	11.446	0.428
68 pre	166.8739	151.731	1.38	4.063	3.144	3.696	0.231
69 pre	119.5729	241.876	1.42	4.067	3.131	4.924	0.6
70 pre	70.0741	470.484	1.342	4.058	3.221	7.22	0
71 pre	153.1371	227.903	1.377	4.042	3.137	4.721	0.404
72 pre	185.823	228.055	1.118	4.068	3.129	4.927	0.399
72 post	31.7	184.5548	172.081	1.322	4.038	3.296	3.143
73 pre	237.0526	143.838	0.663	3.841	3.84	1.231	0.44
73 post	143.1518	442.89	0.96	4.012	3.229	5.726	0.196
75 pre	208.7292	81.533	1.68	4.007	3.281	2.155	0.269
76 pre	96.9955	225.878	1.487	4.083	3.089	4.877	0.438
77 pre	166.992	203.689	1.262	4.2	2.984	5.642	0.482
77 post	224.7342	116.794	1.415	3.275	3.266	1.202	0.687
78 pre	213.8578	220.387	1.094	4.176	3.206	5.012	0.382
79 pre	32.46	54.621	785.621	1.39	4.072	3.169	8.85
80 pre	111.3402	299.432	1.401	4.04	3.199	5.165	0.222
80 post	210.5712	59.703	1.846	3.767	3.526	0.915	0.211
81 pre	55.0404	10000	1.425	4.119	3.006	11.668	0.74
82 pre	182.2439	54.311	1.633	4.233	3.093	2.097	0.407
82 post	9.9422	220.706	0.002	4.645	5.33	0.001	0
83 post	81.7286	1000	1.097	4.111	3.129	10.166	0.241
85 pre	83.4641	535.81	1.441	4.07	3.133	7.378	0.507
85 post	309.6099	32.535	1.784	4.306	3.211	1.316	0
86 pre	282.3578	134.497	1.163	4.113	2.995	4.417	0.361
86 post	124.1585	318.187	1.22	4.17	3.028	6.013	0.242
87 pre	206.2529	96.594	1.708	4.05	3.273	2.629	0.156

Sample ID	UV Pole Amp	Amp	Br	Eo	Eg	Ep	Et
88 pre	182.2017	94.046	1.966	3.757	3.333	1.771	0.27
89 pre	510.2707	0.001	10000	11.076	15	15	15

Appendix B: CompleteEASE User Reference

CompleteEASE is a data acquisition and modeling software made by the J.A. Woollam Company and used in conjunction with their M-2000X model spectroscopic ellipsometer to do the ellipsometry in this thesis. The following guide, written by the author, gives details as to how I used CompleteEASE for SE data collection and developing optical layer models. This guide can help to instruct a user as to how to attain similar results to what were found in this thesis.

Analysis Tab

In this tab, the user employs a building tool and a database of many optical models to build a layered optical model of the sample and fit the model parameters to the experimental SE data. The act of fitting the model to Ψ and Δ spectra is the most important step of ellipsometry, and it is easy to do wrong. Figure 7 shows CompleteEASE open to the Analysis tab with Ψ and Δ spectra for sample #086 pre-annealed loaded and the TiO2(Cauchy).mat model fit to it.

It is very possible to fit model parameters to values that are not correct, but which reduce the MSE significantly and result in a good fit. It is helpful for the user to know the nominal values of model parameters, such as the approximate film thickness or refractive index, and to evaluate with each fitting step whether any parameters have taken on values which are not physically possible. As can be seen in the fit window in Figure 6, the user can generate the model projections based on current model parameter values, but there is also the option to fit model parameters. By right-clicking model parameters, they become highlighted in dark blue and (fit) appears next to them in parentheses.

When you hit the 'fit' button, the selected parameters will be fitted to the experimental Ψ and Δ spectra using a standard, iterative, non-linear regression algorithm (the Levenberg-Marquardt method) to automatically reduce the MSE by altering the fit parameters [CompleteEASE manual citation]. The L-M method does a good job of finding the minimum MSE provided that:

- The optical model accurately represents the sample
- The initial starting values of the fit parameters are reasonably close to their expected values

However, it is possible for there to be variability in the results gained from modeling if one does not pay close attention to how the fitting is done, and what values the model parameters are arriving at. Simply fitting the parameters in a different order will alter the end result.

It is advised to use the simplest model possible that fits the data well. Model complexities, such as surface roughness or refractive index gradients, should only be added to the model if they meaningfully reduce the MSE without causing other issues. In these experiments, a very simple Cauchy model was used for the TiO_2 films. Though it is hard to quantify, in repeated instances of modeling it was noted that the film thickness varied by approximately 4 nm. This variability is due to the many different ways a model can be fit to data. Ideally, one would want to test the uniqueness of a model, by comparing it to the results of many other models, but this is difficult to do in general and in practice.

In order to attain correct estimates of model fit parameters, it is essential that you provide good initial guesses as to what these values are. This can be difficult to do, especially if there is limited literature to call upon as to what those values are. However, one can run into the issue of fitting parameters into a local minimum of MSE, rather than the global minimum of MSE which represents model fit parameters that are physically accurate. For example: If I know my film is more than 100 nm thick then I would never begin fitting model parameters at a film thickness of 50 nm. The fitting algorithm would almost certainly begin fitting the other model parameters around the 50nm thickness, which is not correct, and the other parameters will take on values which are not correct.

To ensure that the fit of your model is accurate and well done, heed these steps:

- Provide good initial guesses for model parameters
- Use the mouse roller wheel to quickly change the value of fit parameters
    - This is an important tool. If you hold the right mouse button over a fit parameter, then the mouse roller wheel can be used to quickly change the value of the parameter and explore how it might affect the fit. Spend some time in between fitting steps adjusting parameters quickly with this tool to get better fitting results.
- In an ideal fit, the model projections lie directly over the Ψ and Δ spectra
    - The whole point of modeling is to get the model projections to lie over the data, so that they are perfectly modeling the Ψ and Δ spectra. Pay close attention to how model parameters can be tweaked to get the projections as close as possible to recreating the Ψ and Δ spectra. It is possible for them to overlap, but for the model to have incorrect fit parameter values that are not physically correct, so be careful
- Lower the MSE

    - The MSE is being used to gauge how close the model projections are to the Ψ and Δ spectra. A lower MSE corresponds to a better fit, so you are seeking to adjust the model fit parameters until the MSE is as low as possible. It is possible to get a very low MSE from improper modeling. An MSE of above 20 is too high and should not be used. An MSE of below 2 is ideal.
- Model fit parameters must be physical
    - It serves to know something about your sample, the relevant optics, and what is reasonable to expect for certain parameter values. In these experiments, I was looking for the following things:
        - Cauchy coefficients A, B, and C cannot be negative
        - B is approximately 0.02, C is approximately 0.006
        - A should be between 2.3 and 2.7
        - Extinction coefficient κ should be near zero
        - IR pole Amp. cannot be negative
- Evaluate how the model fit parameters change after each instance of fitting them
    - Clicking fit in the fit window applies the L-V algorithm to the selected parameters. Every time you do this, you should evaluate whether the fitting step has meaningfully reduced MSE and not caused any model parameters to attain unphysical values. If an error such as that occurs, undo the fitting step and try a different method.

Generally, for the simple models that I created, I relied on the model fit parameters that the models I chose started with as reasonably good initial guesses. In these models, B and C start at 0.02 and 0.006, for example, and using these values allowed me to get good fits. I also took the values of the model fit parameters for the SiO_2 substrate in the CompleteEASE model to be good initial guesses, and will discuss this in the next two subsections. Relying on these initial model parameters may have contributed to not accurately modeling the dispersion of samples, as will be discussed.

Additional Modeling Options

There are a number of additional modeling options that are available to help improve the fit. As is seen in Figure 8, beneath the model building tool are three expandable menus:

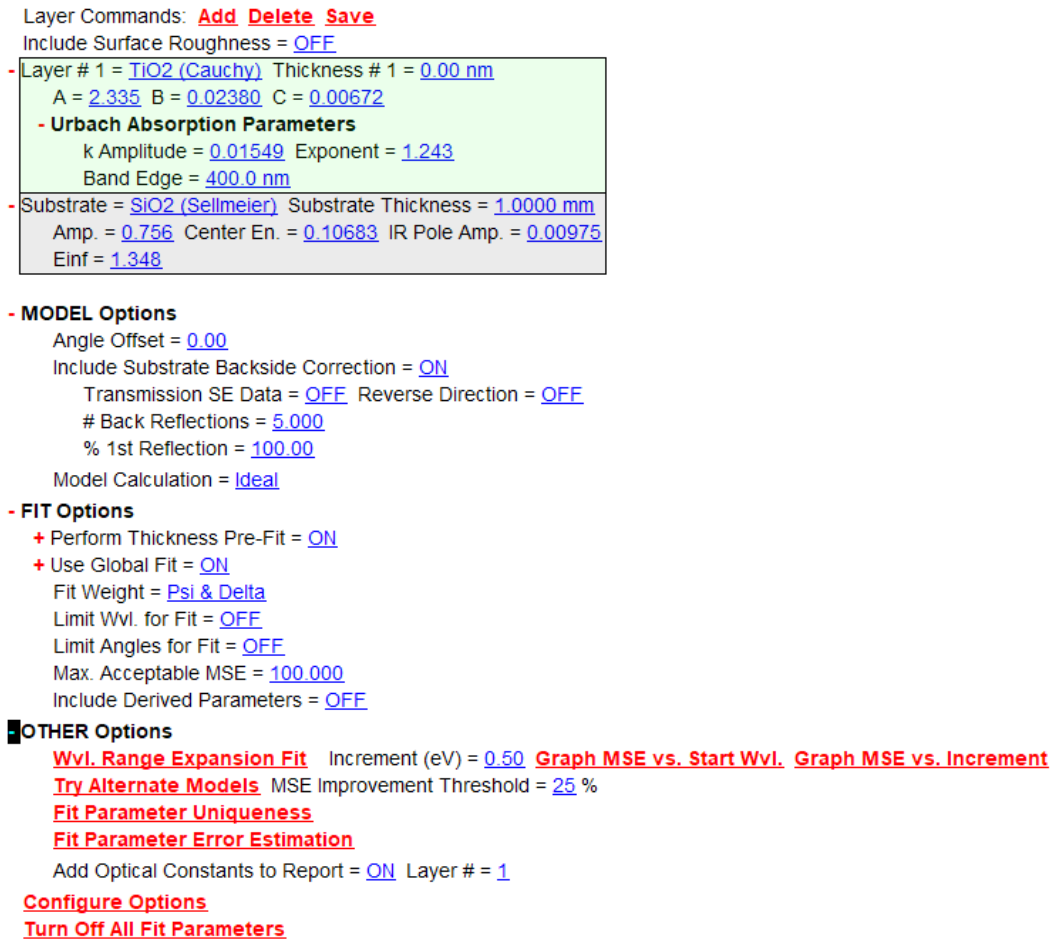

Figure 8: Screenshot of CompleteEASE showing the additional modeling options available in modeling. These are found in the Analysis tab, below the model building tool in expandable menus. The mode building tool is currently displaying the TiO_2 on SiO_2 model.

- MODEL Options
    - The most important option in this menu is Include Substrate Backside Correction. This is a necessary model complexity for TiO_2 films on fused silica. Since this is a transparent film on a transparent substrate (and since the substrate does not have a roughened backside to mitigate specular reflection), the backside reflections off the substrate have to be accounted for. They impact the reflection signal and not accounting for them will alter your results.
- FIT options
    - I kept the Thickness Pre-Fit on. The thickness pre-fit cycles through a range of initial thicknesses, fits them, and chooses the one with the lowest MSE. Global fit

does the same for the initial refractive index. These are tools developed by Woollam to help ensure a good fit to model parameters.

  - In this section you can find the “fit weight”. The fit weight should remain on “N.C.S.”. N, C, and S are useful because they’re bounded between -1 and 1, so their values don’t blow up like Ψ and Δ.

- OTHER options
  - The most important tool in this menu is the Try Alternate Models feature. This will automatically build and apply different variations of the currently applied model. For example, it will show the user the MSE and results from applying surface roughness, index grading, surface roughness & index grading, or by modeling the film as anisotropic. It is worthwhile to see if the MSE is meaningfully reduced by this quick check, but those modeling complexities did not result in dramatically better fits for these results.

Hardware Tab

In this tab, one can access the top-down camera looking at the sample stage. I often used the camera to look at the surface of my sample and translate the sample stage until the beam was hitting a smooth part of the surface. We stored these films on double-sided tape and so both of their surfaces ended up getting dirty and covered in tape glue. With the camera, you can find a spot on the surface that is clearer, and the Ψ and Δ for measuring on such a spot will be much cleaner than if you measure over a dirty spot (the Ψ and Δ lines will be less noisy).

Assorted Advice on Modeling

One simple thing to watch for is the oscillations known as interference fringes in the measured Ψ and Δ spectra. The thicker the film, the more oscillations due to interference from the internal reflections. This effect can be seen clearly in Figure 9:

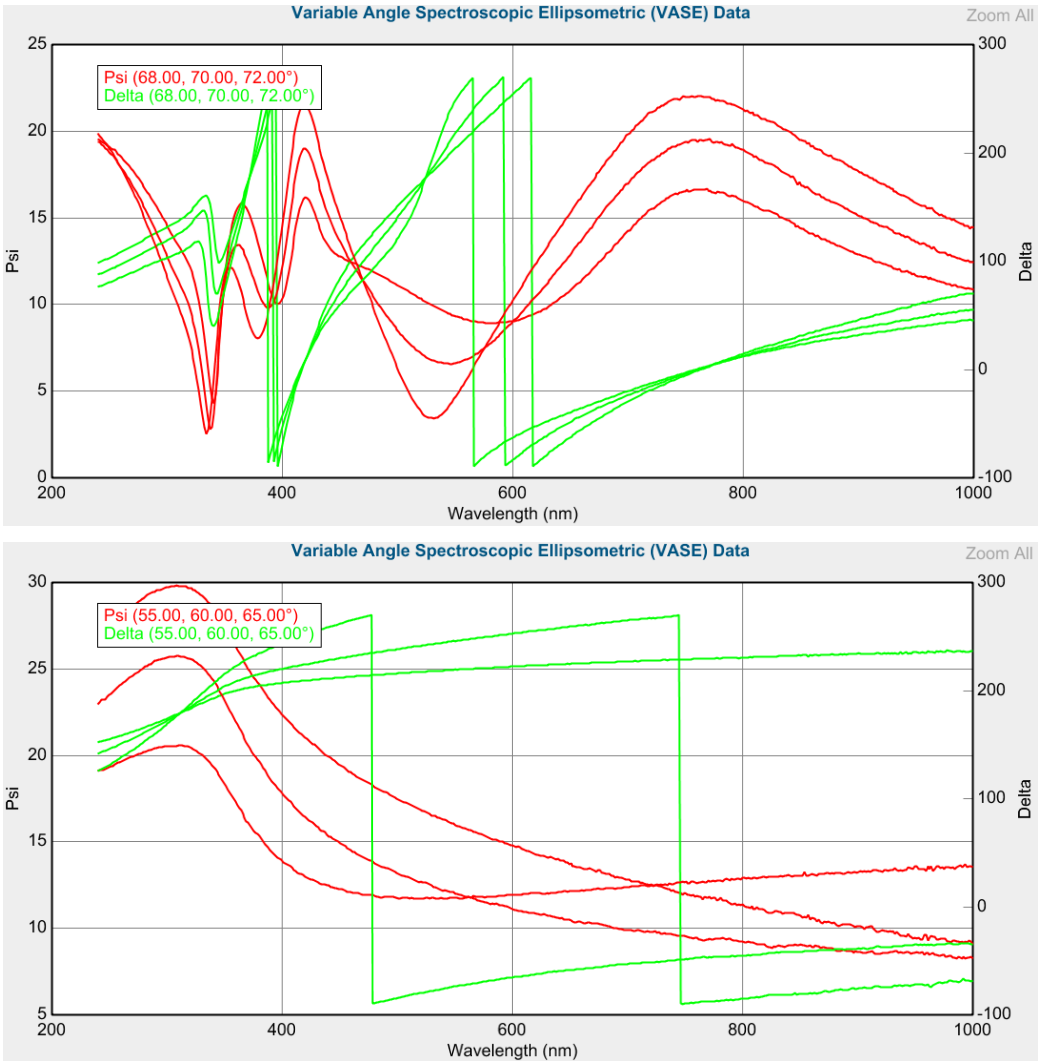

Figure 9: These screenshots show graphs of ψ and Δ spectra for two films. The top graph is the SE data of sample #86 pre, which was estimated to be ~170 nm thick. The bottom graph is the SE data for sample #43 pre, which was estimated to be ~30 nm thick. Note how the thicker film has many more oscillations in the ψ and Δ spectra.